VIRTUAL PELVIC SURGERY SIMULATOR FOR THE PREVENTION OF SURGICAL ERRORS

A THESIS IN

Mechanical Engineering

Presented to the Faculty of the University
of Missouri-Kansas City in partial fulfillment of
the requirements for the degree

MASTER OF SCIENCE

by
MD ARIFUZZAMAN ARIF

B.S. Khulna University of Engineering & Technology, 2014

Kansas City, Missouri
2019

VIRTUAL PELVIC SURGERY SIMULATOR FOR THE PREVENTION OF SURGICAL ERRORS

Md Arifuzzaman Arif, Candidate for the Master of Science Degree

University of Missouri-Kansas City, 2019

ABSTRACT

Recent data suggests that over 200 million surgeries are performed annually worldwide and about 3 to 22% of these surgeries involve some sort of complications. Surgical errors can be caused by both technical errors and cognitive errors which may happen to even an experienced surgeon. Resident surgeons are more prone to surgical errors as they start their surgical career with less experience and skills. In order to quantify the surgical errors and accelerate the learning experience of surgeons, a novel method has been proposed that can identify, model and describe surgical errors by using biomechanical motion analysis and a high-fidelity 3-D surgery simulator. This analysis has been done for a complex, common and high-risk surgery, the midurethral sling (MUS) procedure for stress urinary incontinence. The experimental protocol allowed for monitoring of the surgeon's full body kinematics during the procedure and accurate tracking of the trocar inside the body. Surgeon kinematics and position of the trocar relative to anatomical structures were tracked for both successful (continuous contact with the pubis) and error trials (lateral deviation and cephalad deviation). The kinematics of the wrist, elbow, and shoulder joints demonstrate major differences between the three different passage conditions. Cephalad deviation of the trocar entered the peritoneal cavity, but during lateral deviation, trocar

remains within the anterior side of the pelvic bone without making any contact with the external iliac vein. Off plane rotations of the shoulder, elbow and wrist joints, i.e. abduction-adduction, and internal-external rotations, incurred large errors due to the marker set used in the experiment. The model demonstrated good fidelity except for gel thickness and transparency. Based on the expert surgeon, the physical model replicated the feeling of performing the procedure on a live subject. Differences in the elbow, wrist and shoulder joint kinematics between the three different passage conditions indicate that it is possible to identify errors based on kinematics. Since the kinematics between the different trials seem to be different, there is potential in training novice surgeons on proper kinematics to ensure successful passages of the trocar.

The faculty listed below, appointed by the Dean of the School of Graduate Studies, have examined the thesis titled "Virtual Pelvic Surgery Simulator for the Prevention of Surgical Errors," presented by Md Arifuzzaman Arif, candidate for the Master of Science in Mechanical Engineering degree, and certify that in their opinion it is worthy of acceptance.

Supervisory Committee

Antonis P. Stylianou, Ph.D, Committee Chairperson
School of Computing and Engineering

Gregory W. King, Ph.D
School of Computing and Engineering

Zahra Niroobakhsh, Ph.D
School of Computing and Engineering

CONTENTS

LIST OF ILLUSTRATIONS

FIGURE PAGES

LIST OF TABLES

TABLE PAGES

ACKNOWLEDGEMENTS

There are so many people that I would like to thank who helped and provided support during this project.

To begin, Dr. Stylianou has enabled me to have a fulfilling research experience. He opened the door to a subject that I have become passionate about and challenged me to contribute to this field. Also thanks to my advisory committee members Dr. King and Dr. Niroobakhsh. Also a big thanks needs to go to two co-supervisors of my research project, Dr. Gary Sutkin, and Dr. Gregory King. I would like to thank all my current and previous lab-mates who provided support during my graduate study at UMKC, Dr. Munsur Rahman, Jonathan Parman, Ricky Abnos, and Mohsen Sharifi Renani.

I would also like to thank my family for believing in me and providing support when I needed it. I would like to remember my father who passed away a few months back and without his inspiration and contribution, it wouldn't have been possible for me to come this far. Finally, I am personally indebted to my friends in Kansas City, who offered me love, warmth, and hospitality throughout my life experience in the United States.

CHAPTER 1

INTRODUCTION

Recent data suggests that over 200 million surgeries are performed annually worldwide and depending on the type of the surgery, preventable complications may occur in up to 22% of these surgeries. Even a minor error can lead to serious complications and permanent disability/mortality rates vary between 0.4% - 0.8% (in *WHO Guidelines for Safe Surgery 2009: Safe Surgery Saves Lives* 2009). Surgical errors are often defined as preventable mistakes occurred during surgeries. These errors can be caused by both technical errors and cognitive errors which can happen to even an experienced surgeon. However, resident surgeons are more likely to commit surgical errors as they start their career with less experience and skills. The overall objective of this project is to identify, model and prevent surgical errors in a systematic way. In order to reduce errors and accelerate the learning experience of surgeons, we have used a combination of virtual and physical anatomic models, simulation of surgical errors, and kinematics of surgical instrument and surgeon to describe and define the surgical errors.

This work targets a complex, common, and high-risk surgery for stress urinary incontinence called the midurethral sling (MUS) procedure. The procedure involves using a sharp steel trocar to place a mesh underneath the urethra to control its mobility. For this surgery, the surgeon has to guide the sharp steel trocar blindly past the bladder, bowel and some major blood vessels that require the surgeon to have distinct surgical skills (bimanual dexterity, ability to envision a blind 3-D space, strong knowledge on the complex anatomy

of the periurethral and perivesical spaces etc.) (Skoczylas et al. 2012). The general hypothesis for this study is that: the surgical errors occurred from the surgical instrument passage in midurethral sling procedure can be predicted and prevented by analyzing the kinematics of the surgeon's shoulder, arm, hand and the spatio-temporal characteristics of instrument passage.

This research can lead to effective error prevention by identifying and modeling surgical errors in a systematic way. No surgical error should be ignored as even minor inconsequential error can accumulate into major errors (Gawande et al. 2003; Catchpole et al. 2010; Geraghty et al. 2016). Many of these surgical errors occurring at the operating room are preventable (James et al. 2013) and preventable errors have increased in recent times even though worldwide awareness of the problem has increased as well (Kohn et al. 2000). Young surgeons lack in experience and mastery of skills while they enter into the operating room after their basic surgical training program and there is no technique available to teach them not to commit surgical errors. Kinematic analysis of surgical error can ensure that young surgeons are trained in a better way and surgical errors are kept to an As Low as Reasonably Possible (ALARP) level of safety (Cuschieri et al. 2005). Once this "Kinematic Analysis" method is established based on Midurethral Sling surgery, it can be translated into other surgical procedures as well.

The overall aim of this research project is to create a realistic anatomical platform on which surgical trainees can practice their skills and get effective feedback on their overall surgical errors through kinematic analysis. The objectives or scopes of this research can be summarized as follows:

a. To create a physical and computational platform to perform the Midurethral Sling (MUS) procedure and monitor surgeon kinematics.
b. To determine if the most common error patterns maintain any distinct kinematic profile.

CHAPTER 2

LITERATURE REVIEW

The Institute of Medicine's annual publication (1999) 'To Err is Human: Building a Safer Health System" led to a growing recognition that errors are common in medical practices and also reported how medical errors can harm patient safely (Kohn et al. 2000). No surgical error should be ignored as even minor inconsequential error can accumulate into major errors (James et al. 2013). Many of these surgical errors occurring at the operating room are preventable (Gawande et al. 2003) and preventable errors have increased in recent times even though worldwide awareness of the problem has increased as well (Catchpole et al. 2010). Technical surgical errors are generally associated with lack of surgical experience and can result in poor surgical outcomes, poor patient satisfaction, re-operation and litigation (Catchpole et al. 2010; Geraghty et al. 2016). Young surgeons lack in experience and mastery of skills while they enter into the operating room after their basic surgical training program and there is no such technique available, except Close supervision in the operating room, to teach them not to commit surgical errors. In order to ensure a safer health system, surgical errors should be kept As Low as reasonably Possible (ALARP) level of safety (Cuschieri et al. 2005).

Systems approaches are widely used in high-stake environments, such as aeronautics and aviation, to prevent human errors and are also being used in the operating rooms (in *WHO Guidelines for Safe Surgery 2009: Safe Surgery Saves Lives* 2009). Even though we are living in an era where the culture of safety is encouraged, still the lead

surgeon is mostly responsible for any surgical error occurred (Borchard et al. 2012). Therefore, a large scale error prevention program should be implemented which can focus on improving the skillset of individual surgeon and accelerate the training program (Hanto et al. 2014).

The field of kinematics (generally describes motion in terms of position, velocity and acceleration) can link the surgeon motion during surgical procedure to surgical errors. Previous work has considered gross surgeon movement (Hwang et al. 2006; McBeth et al. 2002; Kirby et al. 2015; Cristancho et al. 2009), but has not focused on correlating surgeon movement with error. High fidelity, virtual and physical anatomic models exist in clinical practices (Varshney et al. 2014), and simulation has also been integrated into these type of models (Wang et al. 2015). However, implementation of simulated virtual model in surgical procedure to improve the surgical skills is yet to be done (Aim et al. 2016; Moglia et al. 2016).

Kinematic analysis of surgical error can ensure that the young surgeons are trained in a better way and surgical errors are kept to an As Low as Reasonably Possible (ALARP) level of safety (Geraghty et al. 2016). Once this "Kinematic Analysis" method is established based on Midurethral Sling surgery, it can be translated into other surgical procedures as well. For this study, one discrete and high-risk step of Midurethral Sling surgery has been analyzed through motion analysis and a pelvic simulator. Midurethral Sling (MUS) is the most common and effective stress urinary anti-incontinence surgery, and about 200,000 stress urinary incontinence surgeries are performed in the United States every year. Moreover, this particular problem is mostly common to the elderly women and

the number of surgeries performed will keep increasing as our population is aging (in *WHO Guidelines for Safe Surgery 2009: Safe Surgery Saves Lives* 2009).

Subject specific virtual and physical 3-D pelvic model developed from a MRI can be combined with biomechanical motion analysis to simulate, model and describe surgical errors quantitatively. High fidelity 3-D anatomical models, developed from CT scans and MRIs, are available (Hassinger et al. 2010, Konchada et al. 2011) and such models can be helpful for surgical trainees to get a better 3-D representation of human anatomy. The aim of this research project is to create a realistic anatomical platform where young surgical trainees can practice their surgical skills and get effective feedback on their overall surgical errors through kinematic analysis. No such research has been done previously that combines development of subject-specific, virtual and physical 3-D pelvic model, and biomechanical motion analysis of surgeon's gross motor movement and surgical instrument movement to identify, model and describe surgical errors quantitatively.

Previously, this type of models, combined with experimental motion capture data, have been developed to analyze knee, shoulder and elbow joint biomechanics (Guess et al. 2012, 2015; Stylianou et al. 2013, 2014; Kia et al. 2014; Rahman et al. 2016). Previously, biomechanical motion analysis has been performed to quantify surgeon movement patterns in endotracheal intubations (ETI) (Siddiky et al. 2015), central venous catheter placement, and laparoscopic trainer usage. Both experienced and novice surgeons performed the ETI procedure and laryngoscope path kinematics were quantified for both of them using motion capture technology. This kinematic analysis suggests that experienced surgeons use finer and more time-efficient maneuvers to accomplish a successful intubation. This type of quantification in the gross motor movement between expert and novice clinicians can

enable us to use training materials more effectively and the progression of novices to experts can be maintained in an effective manner. This research framework can set the platform for evaluation and management of the surgical error in Midurethral Sling anti-incontinence procedure.

CHAPTER 3

BACKGROUND

3.1 Stress Urinary Incontinence

Stress urinary incontinence is a common problem with women that involves leakage of urine while performing daily activities, such as coughing, sneezing, or daily exercise. This problem can affect up to 1 in 3 women which creates embarrassing situation during daily activities. This problem can be treated by following certain strategies, such as performing pelvic floor exercises or modifying lifestyles. But surgeries are often recommended when the above-mentioned strategies cannot cure or improve stress urinary incontinence.

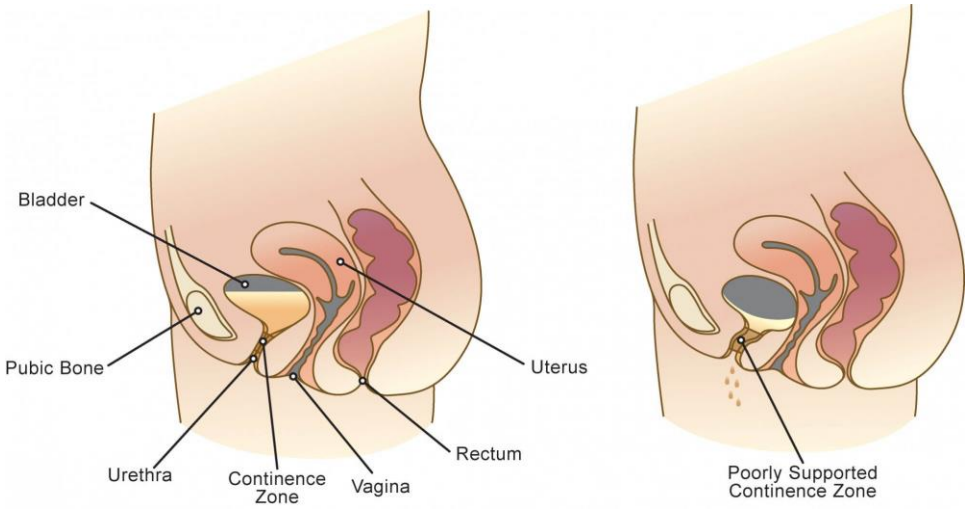

Figure 1. Stress Urinary Incontinence. Source: Caldera Medical (2009).

The urethra serves as the path through which the bladder empties urine. In ideal cases, the muscles and ligaments supporting the urethra can close firmly with straining or exercising and prevent the leakage. These structures can be weakened or damaged with

aging or by child-birth which may result in leakage of urine during straining or exercise, i.e. Stress urinary incontinence. This problem can be treated by placing a sling underneath the urethra which provides additional support to urethra and prevent the leakage of urine. The most common type of sling surgery is the midurethral sling procedure which involves placing of a sling of mesh between the middle portion of urethra and the skin of the vagina.

3.2 Midurethral Sling Surgery

Midurethral sling procedure uses a sling of synthetic mesh underneath the urethra for treating stress urinary incontinence. There are mainly two types of midurethal sling placement procedures available, i.e. 1. Retropubic Sling, and 2. Transobturator Sling. There is another route for placing the sling, i.e. the single incision or mini-sling procedure which is still under investigation. These slings are generally made of polypropylene mesh (open-weave material) which can stay in place without sutures when scar tissue grows around it.

During the retropubic procedure, the sling is positioned underneath the urethra in a U shape. Two ends of the synthetic sling are brought behind the pubic bone and then taken out above the pubic bone through incisions. The retropubic sling procedure is generally referred as the “tension-free vaginal tape” i.e. TVT procedure. This procedure uses a needle-like instrument, called trocar, to insert the sling through an incision in the vagina. This procedure is partially blind, as the sharp steel trocar is guided blindly between the bladder and the pubic bone.

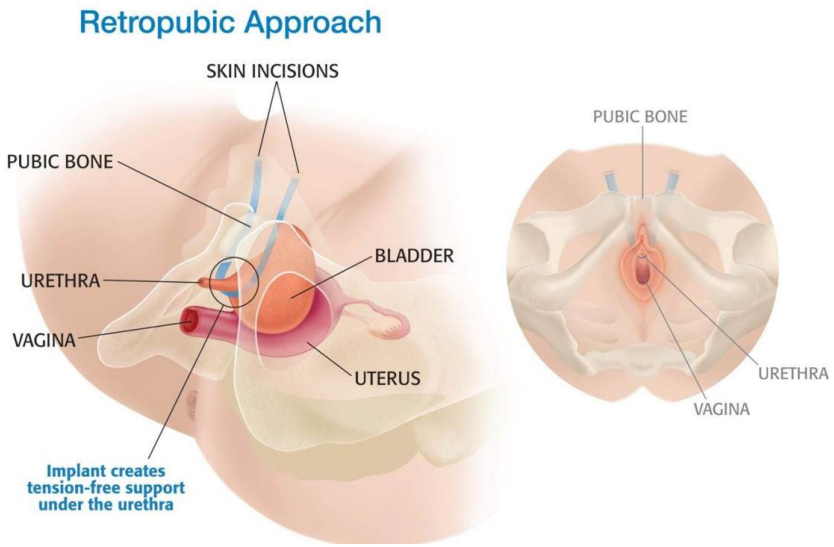

Figure 2. Retropubic Sling Approach. Source: Mahoney & Smith (2014).

In transobturator approach, the sling passes underneath the urethra, but this time the ends of the sling come through two small incisions made in the groin. Both ends of the sling will pass through the obturator foramen (gap between the bones of the pelvis). When the sling is confirmed to be in correct position, two ends of the sling are cut off and skin is closed over them.

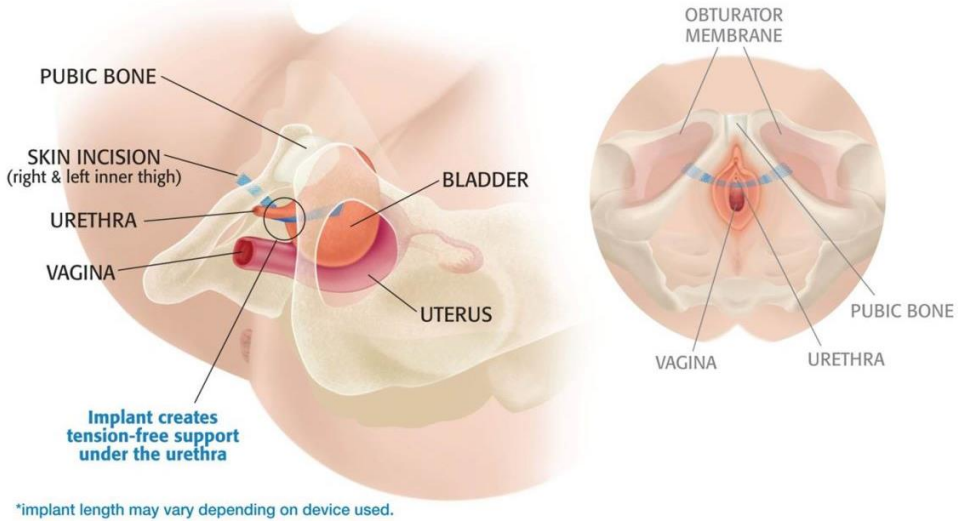

Figure 3. Transobturator Sling Approach. Source: Mahoney & Smith (2014).

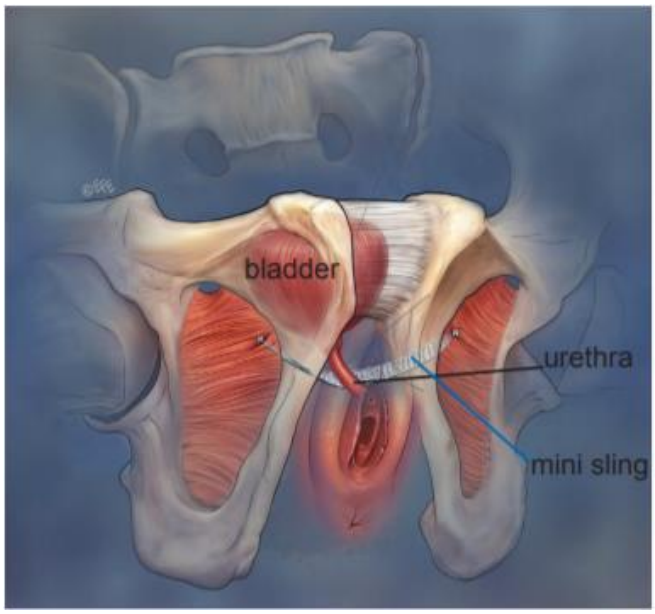

Figure 4. Mini-Sling Approach. Source: International Urogynecological Association (2011).

In mini-sling technique, the ends of sling will not come out onto the skin like the retro-pubic sling procedure, otherwise this procedure has similarity with the retro-pubic technique, at least in the initial part. Here, two ends of the sling are fixed in the correct position with different fixation techniques.

3.3 Surgical Errors Associated with Midurethral Sling Procedure

Recent data suggests that, about 200,000 surgeries are performed every year in the United States for treating stress urinary incontinence. The midurethral sling procedure proves to be a highly successful technique in reducing stress urinary incontinence that involves placing a sling of mesh underneath the urethra. The sharp steel trocar is guided blindly past the bladder, bowel, and some major blood vessels that requires the surgeon to have specific surgical abilities, such as bimanual dexterity, ability to envision a blind 3-D space. The surgeon must possess mastery of knowledge of the complex pelvic anatomy,

specially the anatomy of the periurethral and perivesical spaces. One discrete step of this surgery, insertion of the trocar from the vagina to the suprapubic skin, can lead to disastrous complications. Young resident surgeons are understandably anxious about performing this surgery on patients, as they start their surgical career with less mastery and skills (Skoczylas et al., 2012).

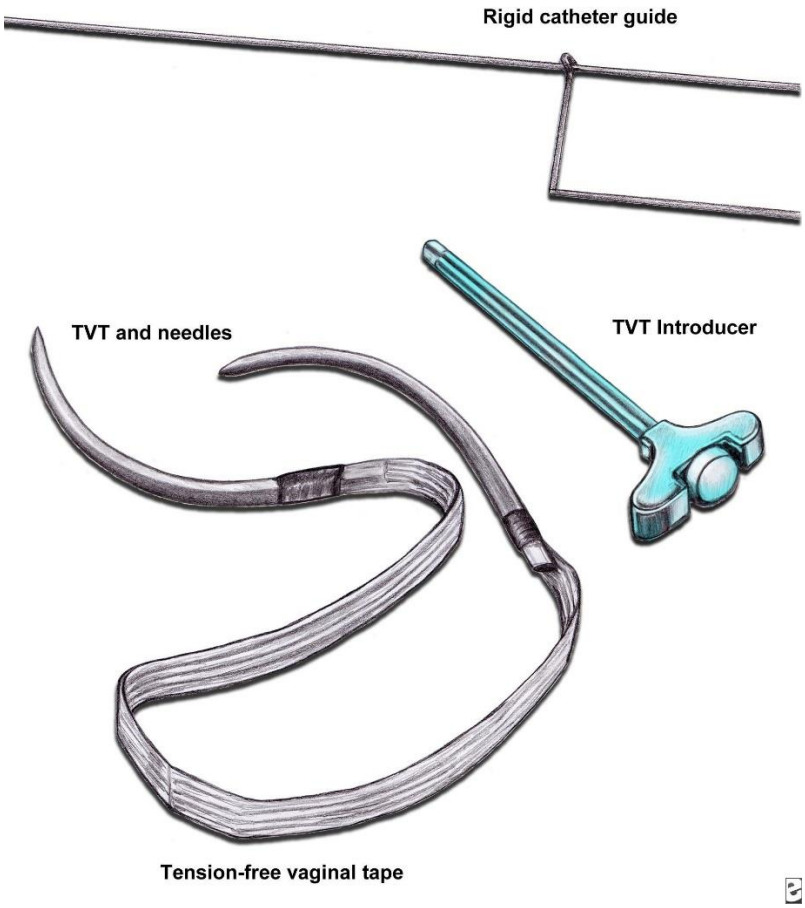

Figure 5. Trocar used in the Midurethral Sling surgery. Source: Vasavada (2018).

If the surgeon fails to guide the trocar appropriately, several complications may occur, including injury to the bladder or urethra (4.9%), injury to the bowel (0.1%), and injury to major blood vessels such as the external iliac vessels (2.0%) etc. (Ford et al., 2015). In addition, incorrect trocar advancement may also lead to other complications, such

as erosion of mesh into the bladder or urethra (0.1%), exposure of the mesh within the vagina (2%) etc. This type of complications may eventually turn this minor surgery into an expensive and prolonged hospital course, requiring blood transfusions, bowel resection, colostomy etc. (Blaivas et al., 2015).

CHAPTER 4

METHODS

4.1 Creation of Virtual Pelvic Model

4.1.1 Magnetic Resonance Images (MRI)

The Virtual Pelvic Model (VPS) was developed from segmentation of high resolution magnetic resonance images (MRI) of a 52-year-old female patient with stress urinary incontinence. MR images of female pelvis were taken at the Saint Luke's Hospital, Kansas City on May 3, 2017 (Figure 1). MRI scans were taken in the sagittal, coronal and axial planes for five different images sequences (T2, Water, Fiesta, InPhase, and OutPhase). MRI Scans were taken on 1.5 Tesla GE Sigma system with a fine resolution setting (0.5 mm slice thickness). Resolution settings for different image sequences are as follows:

Table 1: Resolution settings of MR sequences

Sequence	TR	TE	EC
T2	2500	138/Ef	1/1, 83.3kHz
Water	3.7	1.7	1/1, 142.9kHz
Fiesta	4.3	1.6/Fr	1/1, 125kHz
InPhase	3.7	2.2	142.9kHz
OutPhase	3.7	1.1	1/1, 142.9kHz

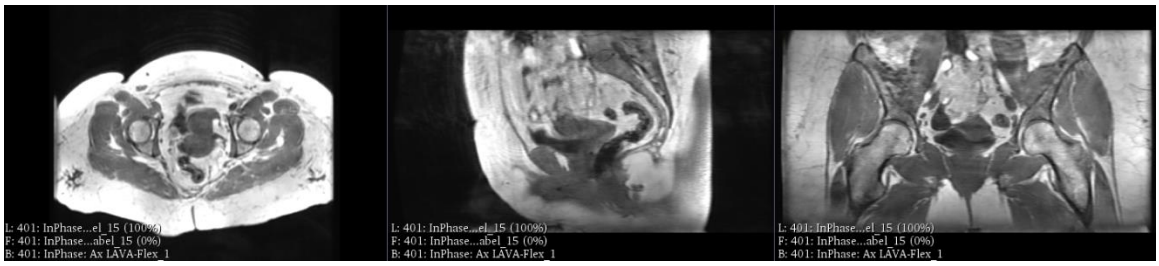

Figure 6: Pelvis MRI (InPhase sequence)

4.1.2 MRI Segmentation

MR images of female pelvis were segmented using 3D Slicer (www.slicer.org). High resolution T2 MR Image sequences were used to segment the bowel, urethra, vaginal wall, ureter, levator muscle and rectus abdominus muscles. Muscles such as obturator, quad, vastus, adductor, tensor fasciae latae, sartorius, iliopsoas, rectus femoris, piriformis, pectineus, gracillis, semimembranus and semitendinosus were more clearly visible from out-phase MR image sequences. In-Phase MR image sequences were used to segment the skin (with fat layer), part of bowel and urethra. Major blood vessels (external iliac vein and artery, femoral vein and artery), fascia and bowel were segmented from the Water MR Image sequences. Femur, pelvic bone, bladder, rectum and uterus were segmented from all five sequences (T2, In-Phase, Out-Phase, Water and Fiesta) and merged to finalize these geometries.

High resolution Out-Phase MR image sequences have been used to extract the peritoneum membrane which can be used as an indicator of surgeon's performance. In ideal cases, it is expected that the surgeon will maintain a distance between the trocar tip and peritoneum membrane while performing this surgery. After segmenting individual geometries, Model Maker algorithm in 3D slicer was used (with smoothing and decimation parameter of 0.20 and 0.25 respectively) to create the shell model of all the segmented

geometries. This helps to visualize the segmented structures and correct them with correct anatomical orientation.

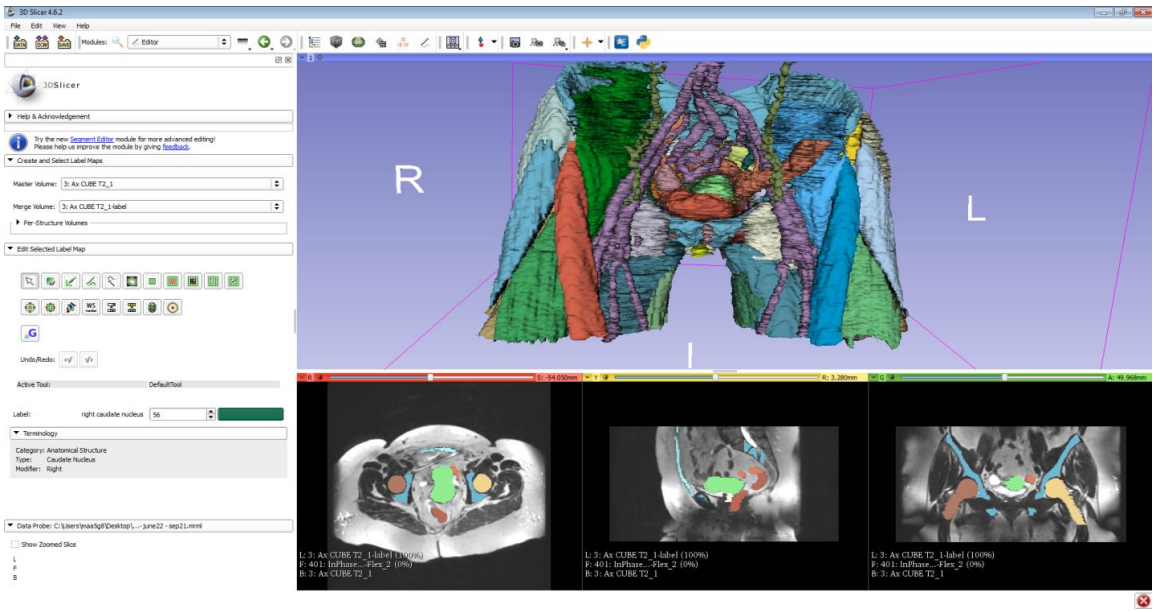

Figure 7: Segmentation in 3D Slicer

Both manual segmentation and automated segmentation techniques have been used to segment the MR images of female pelvis. A Wacom Cintiq 12wx Interactive Pen Display (Wacom Company, Ltd., Tokyo, Japan) tablet has been used to segment the structures manually. Manual segmentation has been mostly used because of the non-uniform boundary thickness and intensity of different soft tissue structures in pelvic MRI (such as blood vessels, urethra etc.). Auto segmentation tools in 3D slicer, such as Robust Statistics Algorithm and grow-cut algorithm, have been used for the structures that show homogeneity in intensity and boundary thickness throughout the length of the structure (such as femur, bladder, uterus etc.). Auto segmentation parameters used for femur in Robust Statistics algorithm are as follows:

- Approximate Volume (mL) – 250

- Intensity Homogeneity – 0.25
- Boundary Smoothness – 0.25
- Max Running Time (min) – 10

Output label volume, original image, label image and output volume have been selected accordingly. All the segmented geometries have been exported as .stl files and taken for further post-processing.

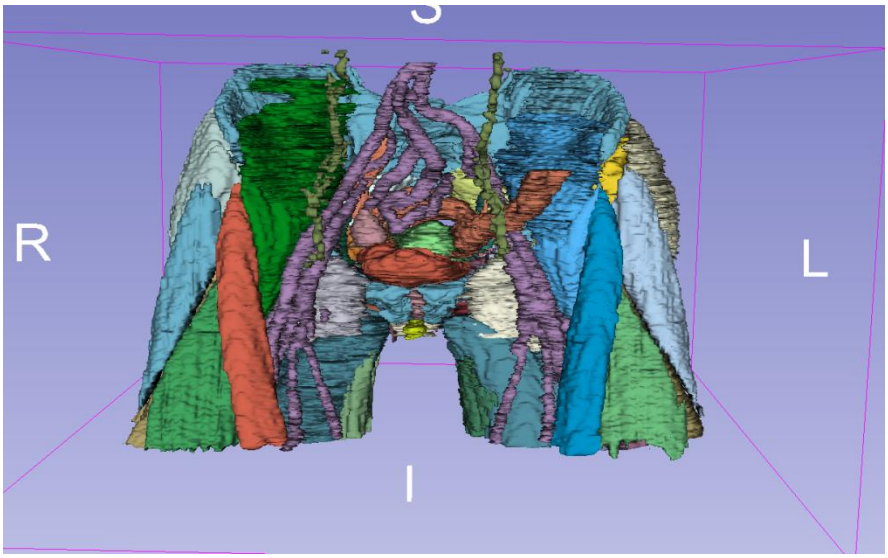

Figure 8: Geometries exported from 3D slicer

4.1.3: Post-Processing

The 3-D geometries exported from 3D slicer were post-processed using MeshLab (http://www.meshlab.net/) and Artec Studio (www.artec3d.com). Post-processing of 3-D geometries included reduction of artifacts and noise, and decimation to reduce the file sizes. Reduction of noise has been used to smooth the jagged features caused by the manual segmentation process. Decimation of the geometries can reduce the polygon count of the geometries and thus provide the geometry with a suitable file size. Once post-processed, exported geometries provided smooth and real-like representations of the organs.

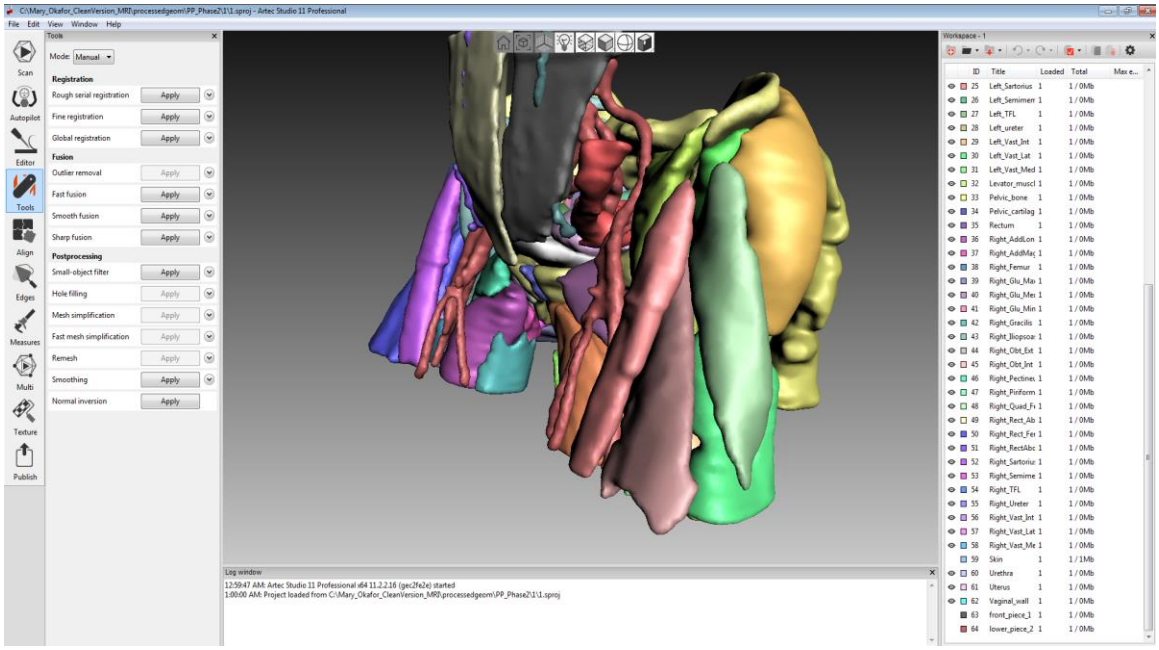

Figure 9: Post-processing in Artec Studio.

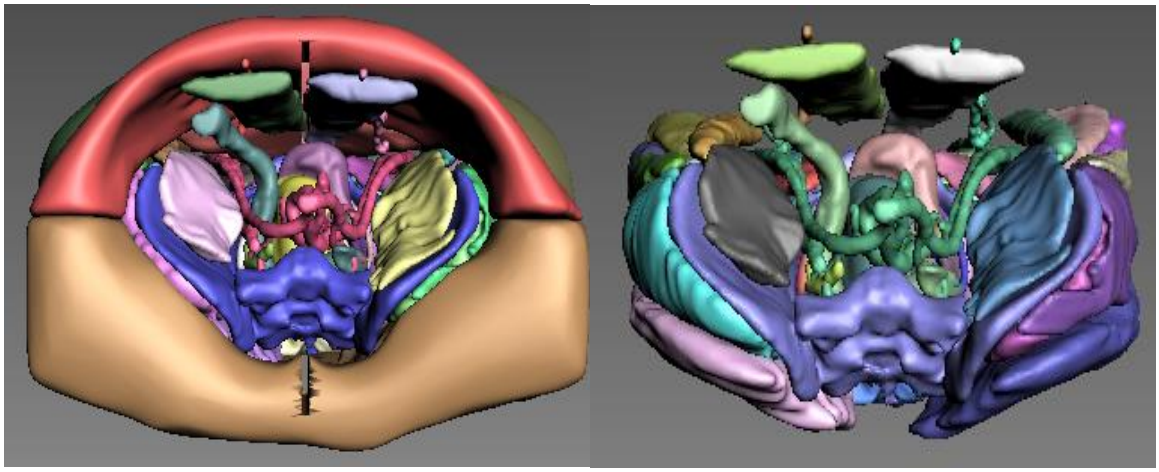

Figure 10: Pelvic Model (after post-processing)

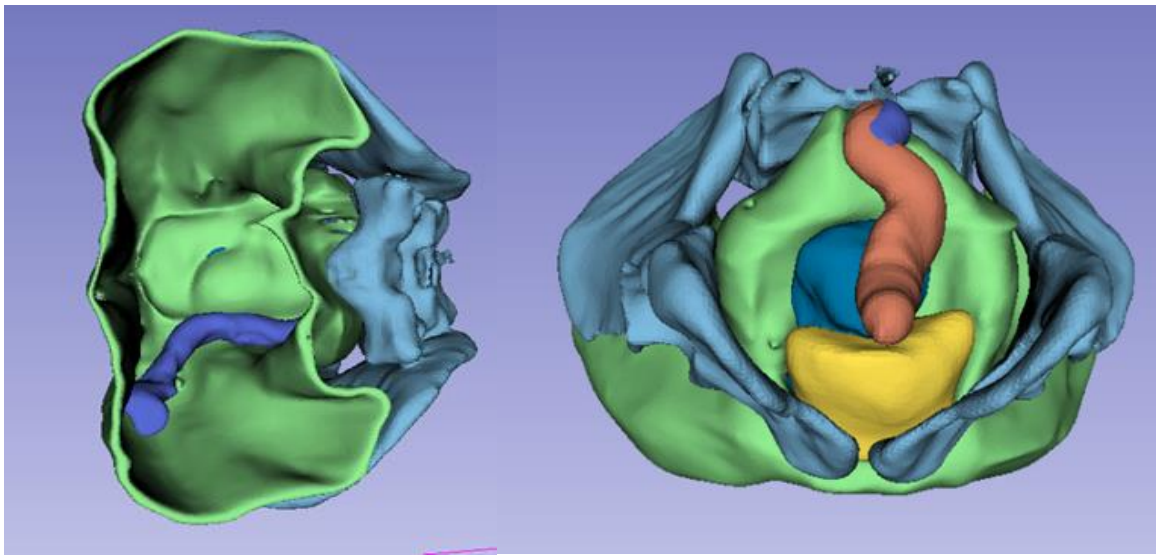

Figure 11: Pelvic Model with Peritoneum

4.2 Creation of Physical Pelvic Model

4.2.1: Computer Aided Design of simplified physical model & printing

The physical pelvic model was manufactured by 3-D printing the geometries from virtual model using a Dimension bst1200 series 3D printer. Vaginal skin was not clearly visible in the pelvic MRI, so it was scanned from an external source using EVA handheld 3D scanner and adjusted to the virtual pelvic model with respect to the anatomic position of urethra. A simplified physical pelvic model was developed in solidThinking module of Altair Inspire^{TM} (https://solidthinking.com/), considering only a part of the pelvic bone and vaginal skin. This model basically serves as a two-part mold where the removable part has been merged with the vaginal skin surface. End wall of the physical model has been adjusted considering the outer surface of the bladder and peritoneum membrane. This end wall serves as the boundary line where the tip of the trocar should never reach.

Figure 12: Physical model filled with ballistic gel

4.2.2: Preparation of ballistic gel

ABS plastic has been used to manufacture the physical pelvic model and the space in between the layers has been filled with a specific kind of ballistic gel, PERMA-GEL (PERMA-GEL Inc., Oregon, USA). PERMA-GEL is a synthetic, clear, and non-toxic material that can serve as a "soft-tissue" medium for this kind of testing. Steps followed to create the soft tissue medium are as follows:

- A roaster oven has been used to melt the raw base media of PERMA-GEL. Small blocks of gel (1-1/4 inch) were sliced from one end of the raw gel block (approximately 5×11×17 inches) and taken to a pan for the melting process. Dry rug was used to clean the oven and no water drop or perspiration was allowed to stay as it could result in the formation of bubbles.
- Gel blocks were melted at around 200 F temperatures on roaster oven and it took approximately 4 hours to complete the melting process. Gel temperature was measured by inserting a thermometer into the gel at about 1 inch distance from the

corner of the pan. The gel temperature should not exceed 300 F to maintain the quality of the gel during recycling.

- Molten gel was then poured into the mold through a hole made using a hand drill. The removable part was firmly fixed with the other part of the mold to prevent the molten gel from leaking out. After pouring the molten gel, the mold was cooled for about 16 hours and then the removable part was carefully removed from the solidified gel block.
- A heat gun was used to remove the bubbles from the surface of the gel block and finally the physical model was prepared for the experiment session.

4.3 Motion Capture Analysis

4.3.1: Experimental procedures

OptiTrack Motive passive marker tracking system (NaturalPoint, Inc., Corvallis, OR) has been used to measure the kinematic characteristics of surgeon and instrument. The physical model was placed on a table firmly by fixing its base with clamps. Assembled trocar and T-handle instrument were scanned to obtain geometries for later use in virtual pelvic model. A cluster of total 7 markers was placed in the trocar to measure the instrument kinematics. 3D positions of the trocar tip and reflective marker were digitized using an Optotrak Certus infrared active marker tracking system that enables virtual tracking of the trocar tip trajectory during the passage of the sling. Five additional markers were placed on the physical model to locate the pelvic geometries in the experimental coordinate system.

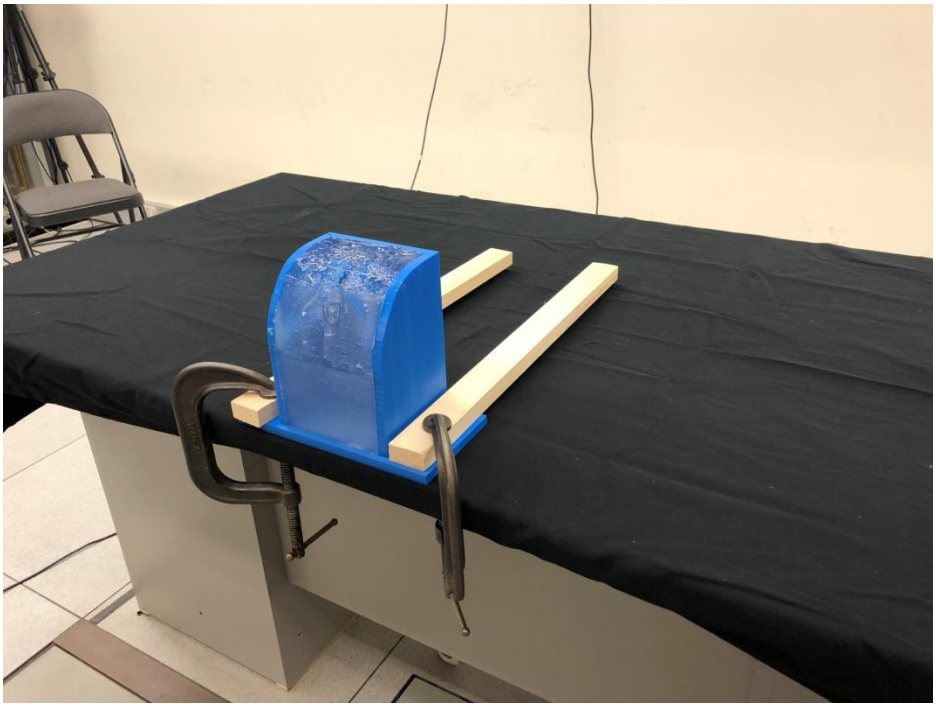

Figure 13: Experimental setup of the physical pelvic model

4.3.2: Surgeon and Instrument Kinematics

An experienced surgeon with more than 20 years of surgical experience performed the midurethal sling procedure on the physical pelvic model. A total of 25 reflective markers were placed on the upper extremity of the surgeon using an OptiTrak motion capture suit. Reflective markers were placed on surgeon's upper extremity in a custom configuration to facilitate optimum motion data capture. The surgeon performed total eight simulated trials of the MUS procedure on the physical pelvic model, including 6 control trials and 2 error trials. The surgeon intentionally makes contact of the end wall (i.e. edge of the bladder) with the surgical instrument while performing the error trials. The OptiTrack motion capture system records the 3D positions of the markers placed on the surgeon and surgical instrument.

Figure 14: Surgeon making tunnel before inserting sling

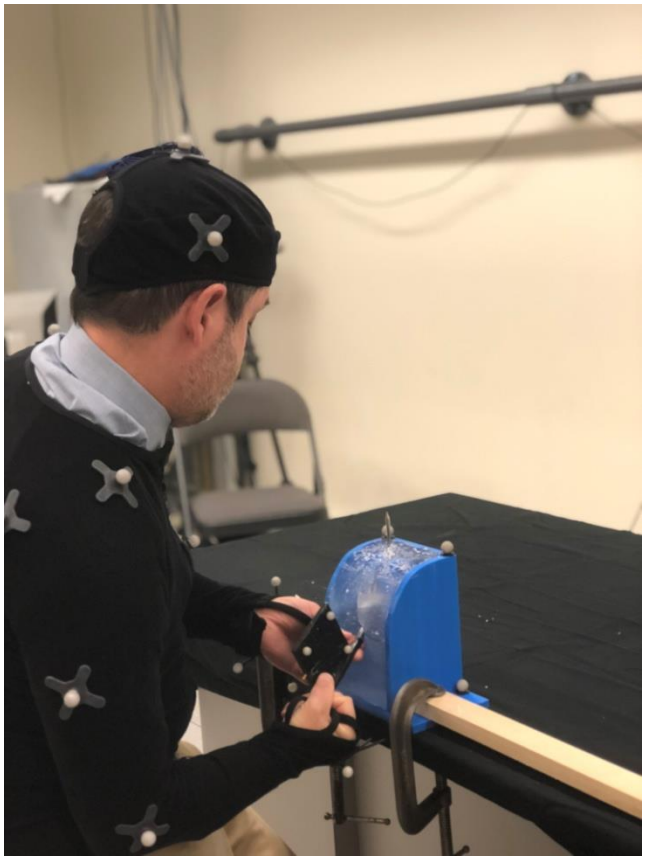

Figure 15: Surgeon performing MUS procedure.

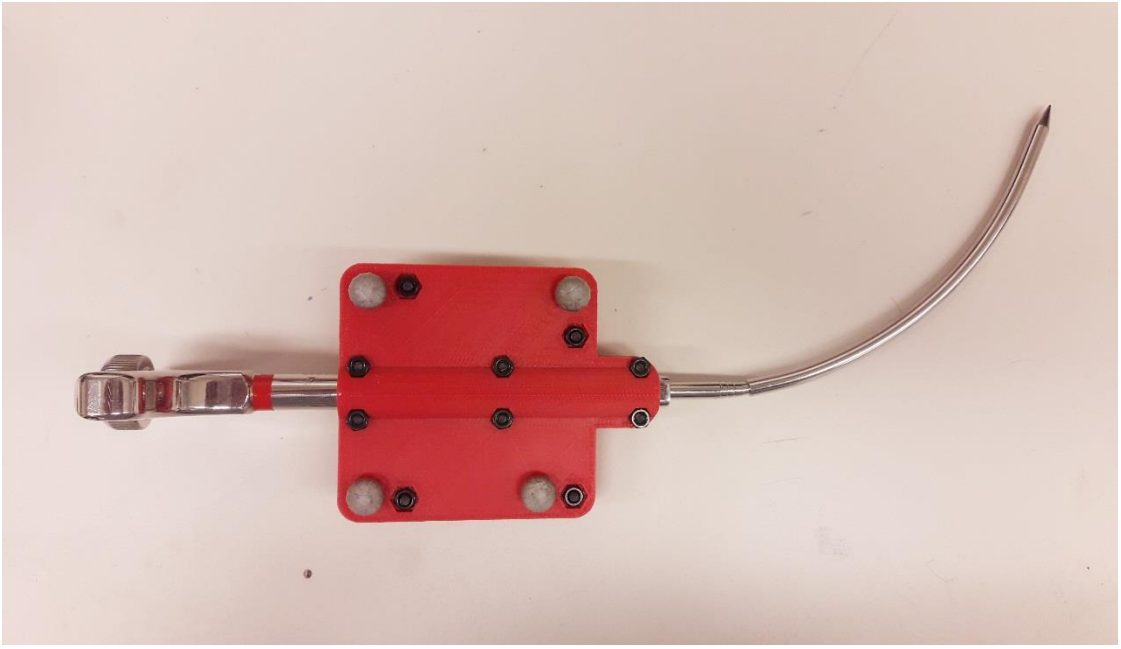

Figure 16: Modified Surgical Trocar with Reflective Markers

4.4 Virtual Pelvic Model in ADAMS

A computational model was developed in MSC ADAMS (MSC Software Corporation, Santa Ana, CA) by importing the geometries segmented from pelvic MRI, experimental model geometry, scaled skeleton geometries, and trocar geometry. The geometries were aligned to the experimental position using the initial position data collected during the experimental procedure.

4.4.1 Skeleton Scaling

Skeleton geometries from a previously developed computational Bio-model (Stylianou et al.) were scaled and fitted to a subject specific skeleton model. Biomech (57) marker placement (OptiTrack Motive) and Plug-in-Gait Marker Placement (VICON) have been compared to determine the markers common in both marker placement system, especially the markers placed in the bony landmarks. Joint center coordinates and the bony landmark marker coordinates were mainly used to calculate the scaling factors for all the skeleton segments and thus obtain the subject specific skeleton geometries. A custom built macro was used in MSC ADAMS to scale and import the geometries to the ADAMS Bio-model. Scaled skeleton segments were aligned to the experimental position using the initial position data from OptiTrack Motive motion data for each experimental trial.

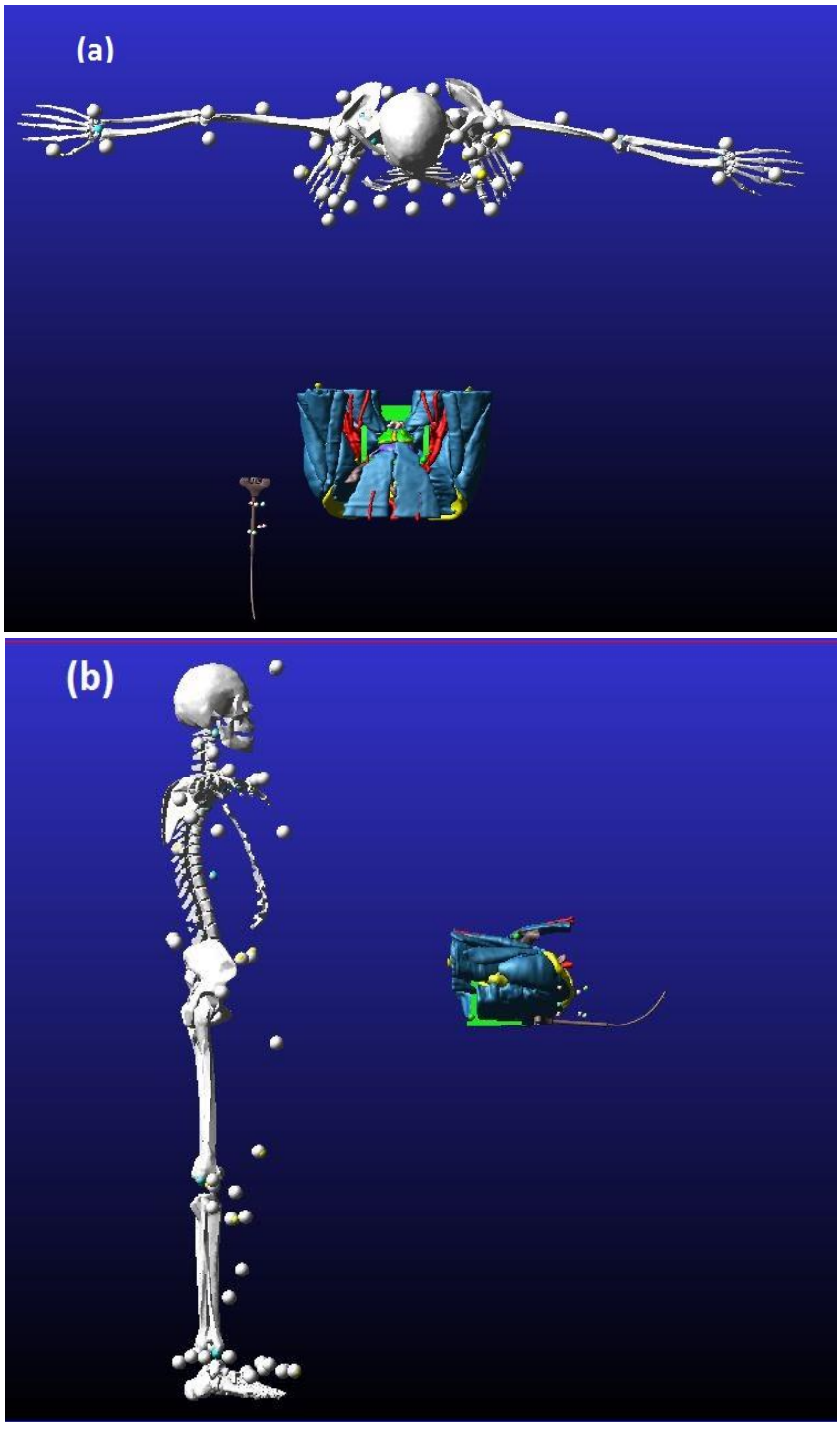

Figure 17: Computational model aligned at the initial static T-pose position in experimental testing, (a) Top view, and (b) Right had side view.

4.4.2 Computational Model Creation

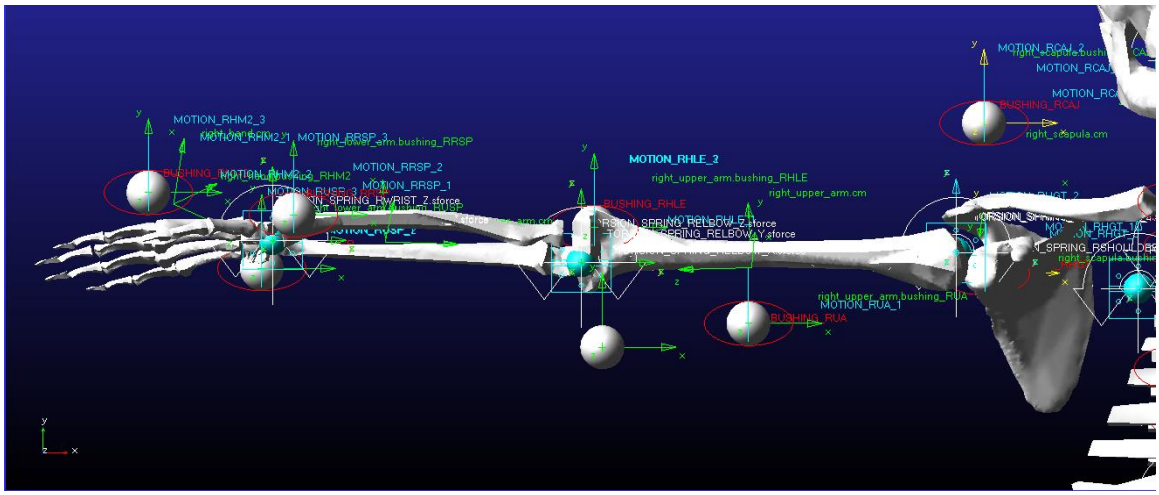

Figure 18: Multi-body model of the right hand in ADAMS

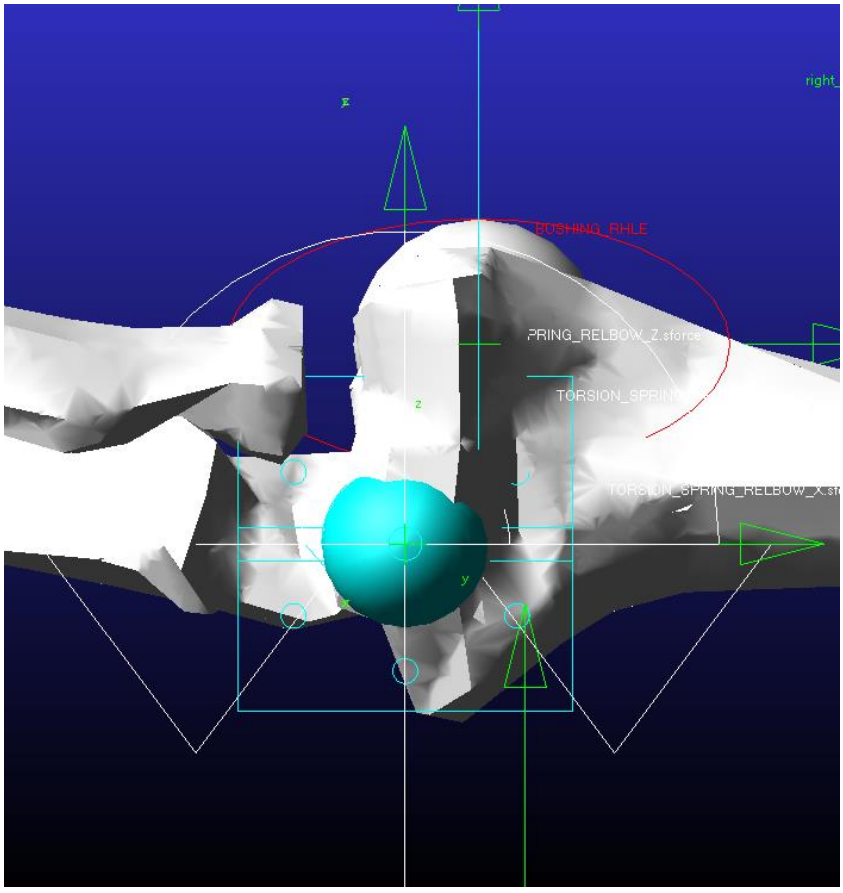

Figure 19: Elbow joint in ADAMS Model

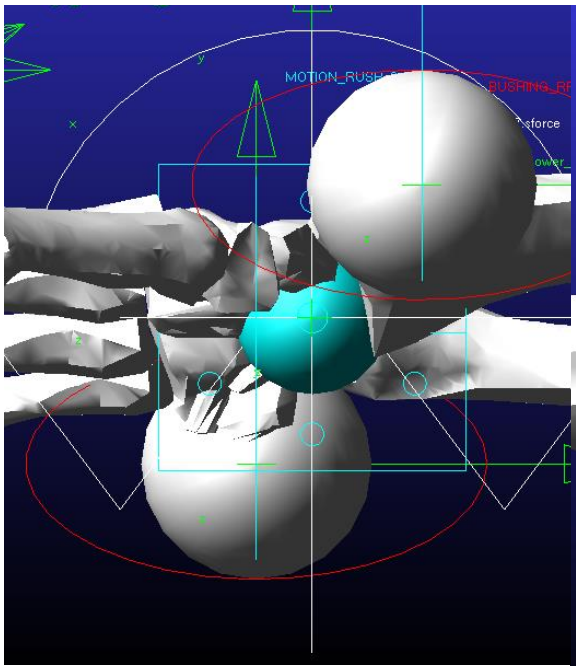

Figure 20: Wrist joint in ADAMS model

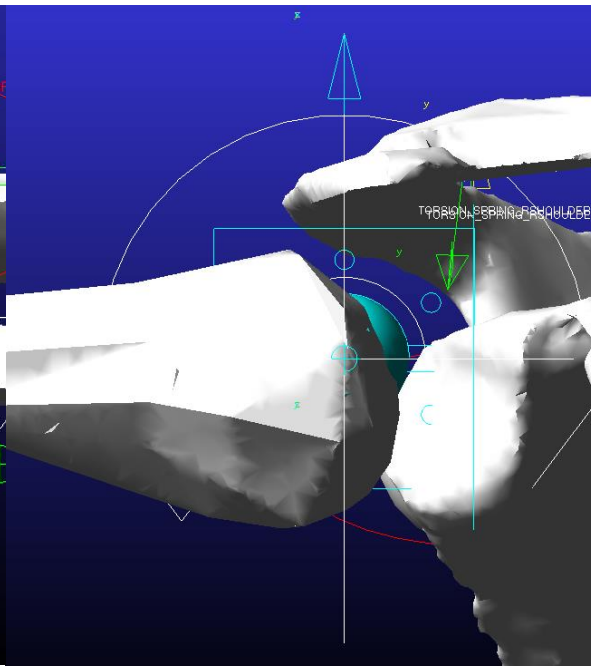

Figure 21: Shoulder joint in ADAMS model

The joint locations obtained from the motion capture data serve as the BASIS markers for body segments. To create the joints, dummy parts are created for each joint and then the joints and torsion springs are created for each revolute joints. ADAMS's precision movement utility has been used for the fine adjustment or alignment of the geometries relative to the corresponding marker's initial (static T-pose) locations from experimental data. Motion capture (MOCAP) ellipsoids were created at the locations of the Biomech (57) plugin markers on the body segments. To apply motion, motion agents were created in the same locations as the body segment markers and they were connected to the body segments with bushings.

Custom macro files have been written to import geometries, assign mass and inertia properties, create MOCAP markers at the average static T-pose location, create ellipsoids on body parts at MOCAP locations, create state variables, create revolute joints, create

motions and to create measures around X, Y and Z directions. This model can calculate rotations around X, Y and Z directions which denote internal-external rotation, abduction-adduction and flexion-extension angles for individual joints. Here, X corresponds to the frontal axis, Y corresponds to the sagittal axis and Z corresponds to the transverse axis. Individual computational model was developed for each experimental trial and simulated using corresponding motion data obtained from OptiTrack Motive.

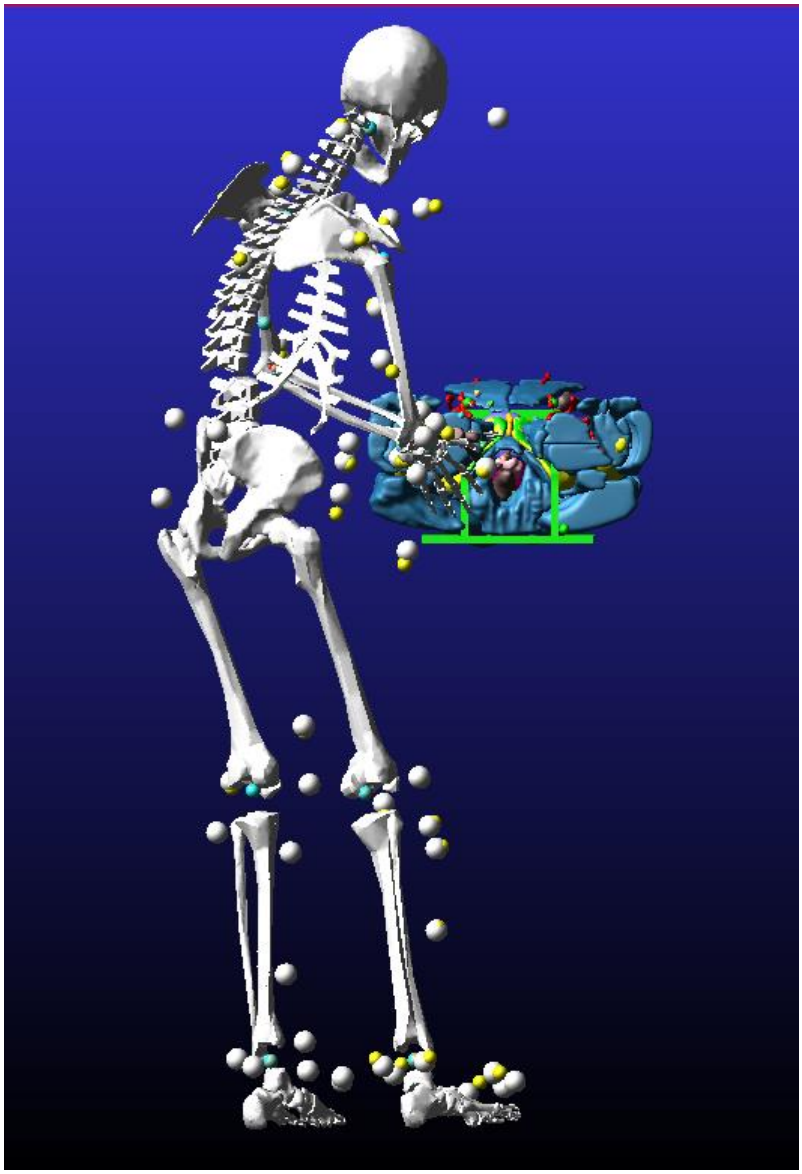

Figure 22: **C**omputational model using surgeon motion data captured with OptiTrack Motive

CHAPTER 5

RESULTS

5.1 Kinematic Analysis

The Virtual pelvic model was combined with the kinematic data obtained from the experimental procedure, and simulated for both successful and error trials. The OptiTrack Motive motion capture system was used to capture the motion data for 3 different trials.

Trial 1: Error-free (successful) passage of the trocar (Continuous contact with pubis)

Trial 2: Surgeon tries to puncture the iliac vein (Lateral Deviation),

Trial 3: surgeon tries to puncture the bowel (Cephalad Deviation).

For this particular experimental setup, an expert surgeon intentionally tries to replicate the error trials and flexion-extension angles have been reported here for both error-free (success) and error-trials. Total trajectory of the surgical trocar has been divided into 3 distinct phases based on the relative positon between the trocar tip and the pelvic bone. These three distinct phases of the procedure are as follows:

Phase 1: trocar passage from skin to inferior side of the pelvic bone,

Phase 2: trocar passage from inferior to anterior side of the pelvic bone,

Phase 3: from anterior side of pelvic bone to end.

Flexion-Extension angles were calculated from the computational model for both right and left elbow, shoulder and wrist joints during the-3 phases of the procedure.

5.2 Surgeon and Instrument Kinematics Simulation

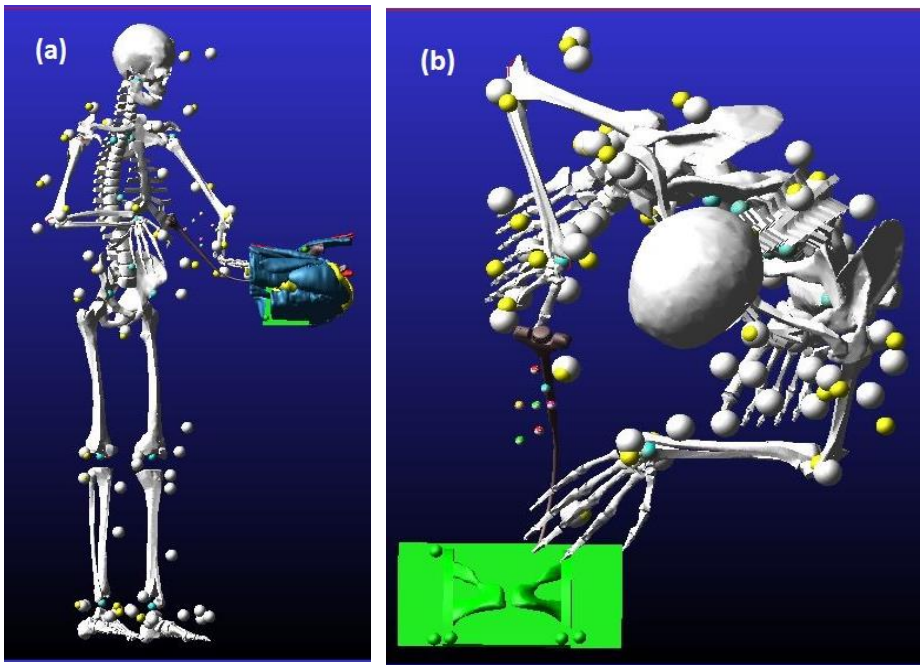

Figure 23: Error-free (Success) trial: Trocar passage starts from skin (a) Surgeon kinematics, (b) Instrument kinematics

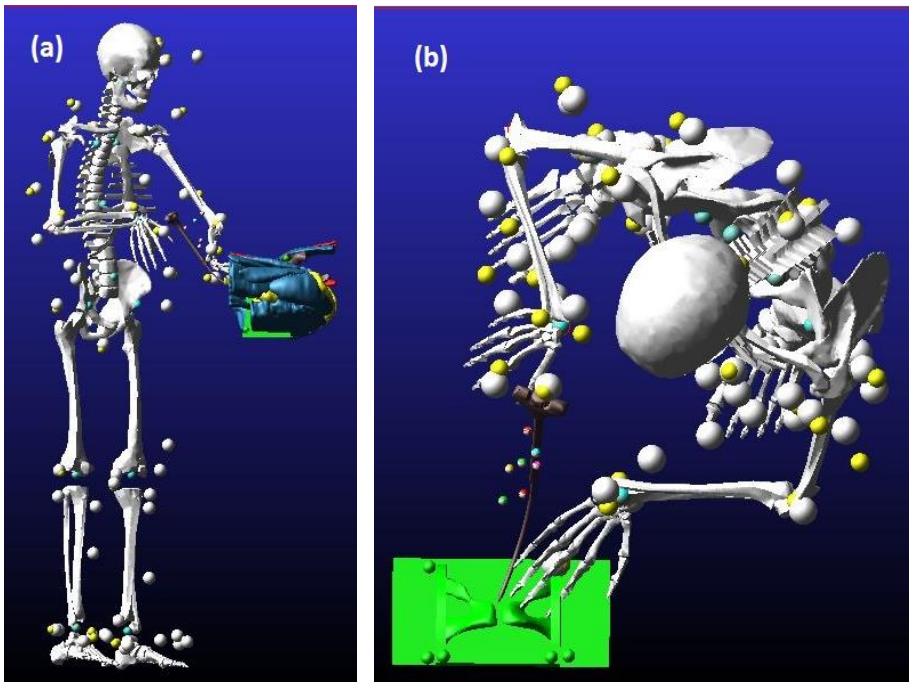

Figure 24: Error-free (Success) trial: Trocar reaches the inferior side of pelvic bone (a) Surgeon kinematics, (b) Instrument kinematics

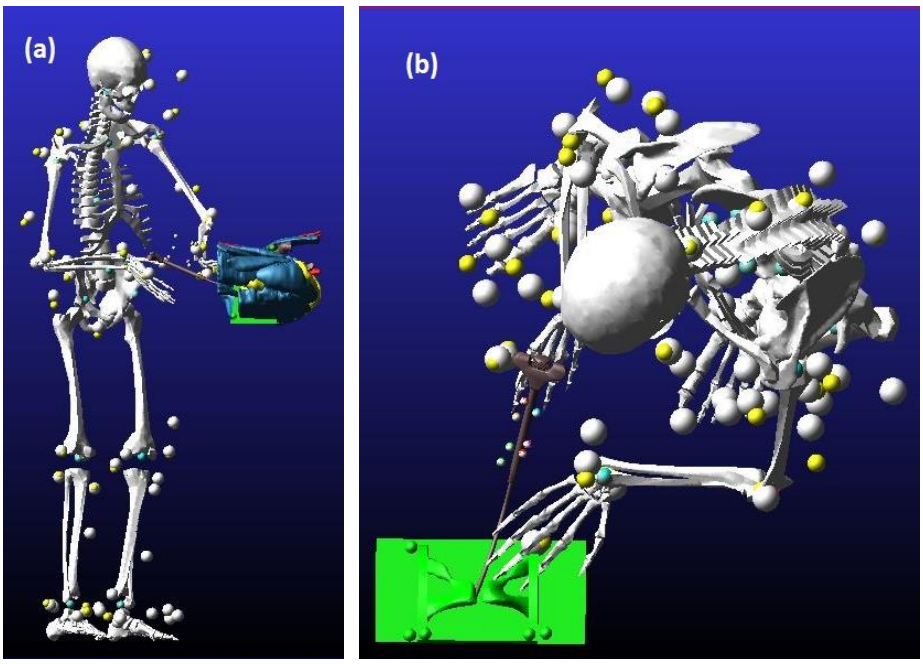

Figure 25: Error-free (Success) trial: Trocar reaches the anterior side of pelvic bone (a) Surgeon kinematics, (b) Instrument kinematics

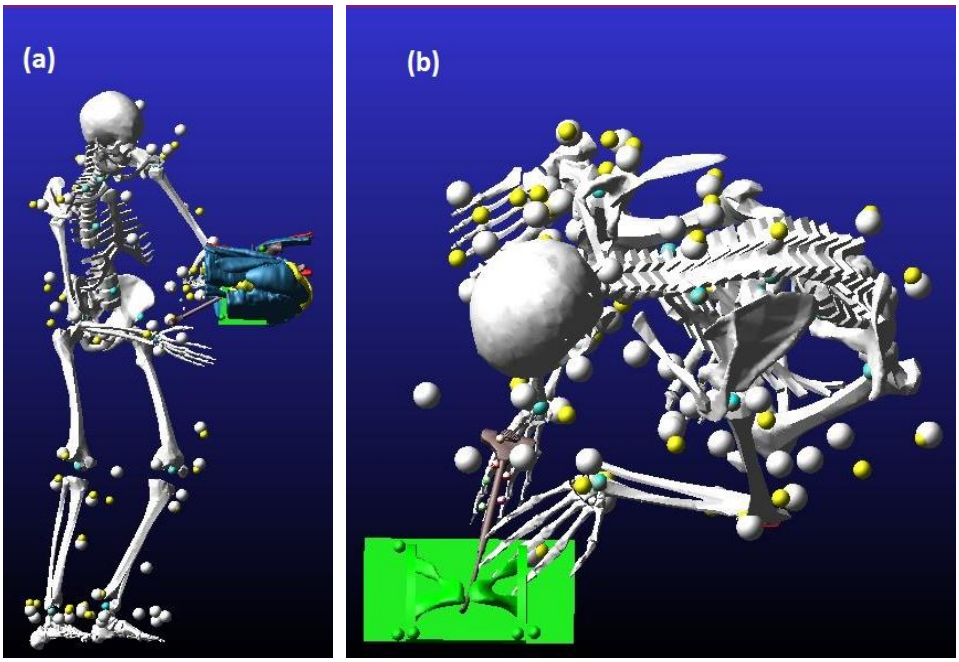

Figure 26: Error-free (Success) trial: End of trocar passage, surgeon releases the trocar (a) Surgeon kinematics, (b) Instrument kinematics

Figures 23-26 show the surgeon and instrument kinematics for error-free (success) trial at 4 distinct time steps. Trocar passage starts from vaginal skin at time step-1 as the surgeon starts guiding the trocar through the vaginal skin and phase-1 starts (Figure 23). Trocar reaches the inferior side of the pubic bone at time step-2 and phase-1 ends at this point (Figure 24). Surgical trocar reaches the anterior side of the pelvic bone at time step-3 and phase-2 ends at this point (Figure 25). Trocar reaches the end point of the procedure at time step-4 (Figure 26) and the surgeon releases the surgical instrument at this point. This point marks the end of retropubic trocar passage.

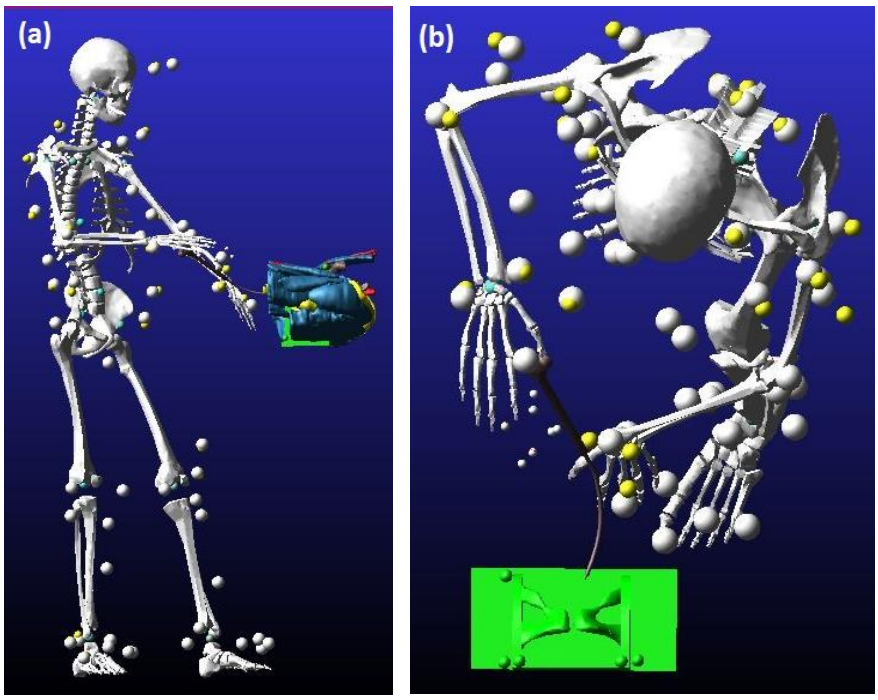

Figure 27: Cephalad deviation: Trocar passage starts from skin (a) Surgeon kinematics, (b) Instrument kinematics

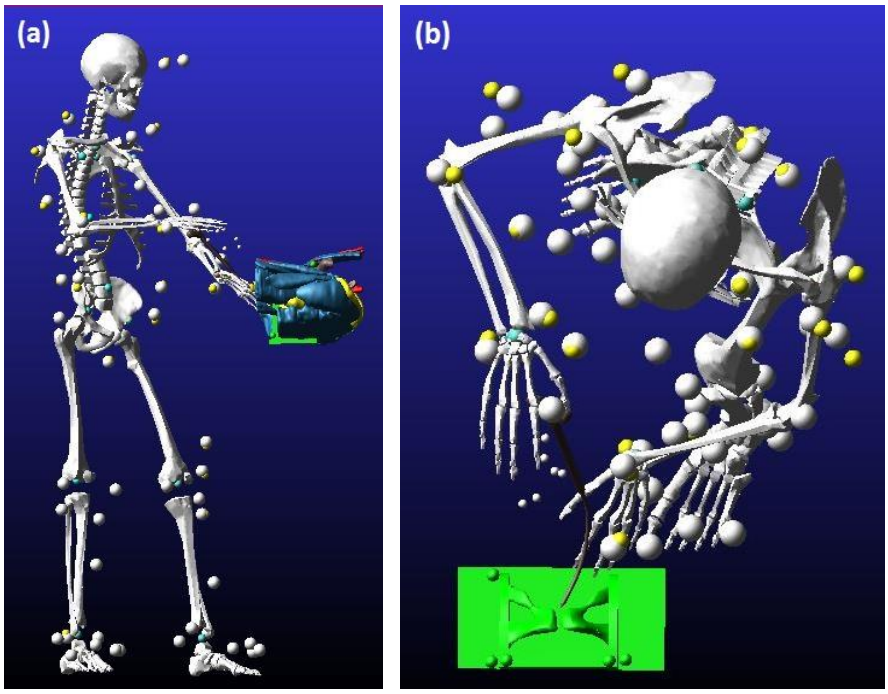

Figure 28: Cephalad deviation: Trocar reaches the inferior side of the pelvic bone (a) Surgeon kinematics, (b) Instrument kinematics

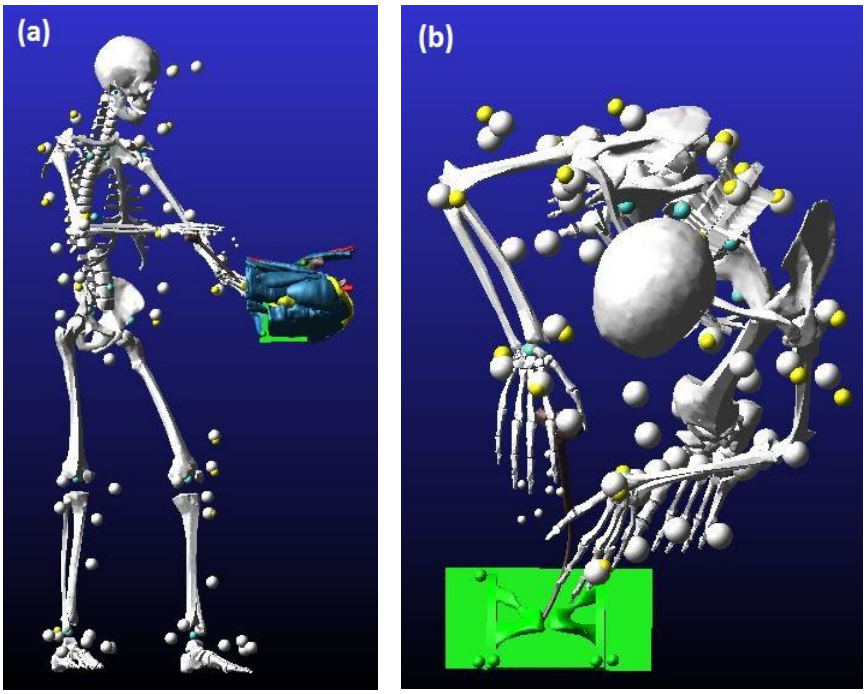

Figure 29: Cephalad deviation: Trocar reaches the anterior side of pelvic bone (a) Surgeon kinematics, (b) Instrument kinematics

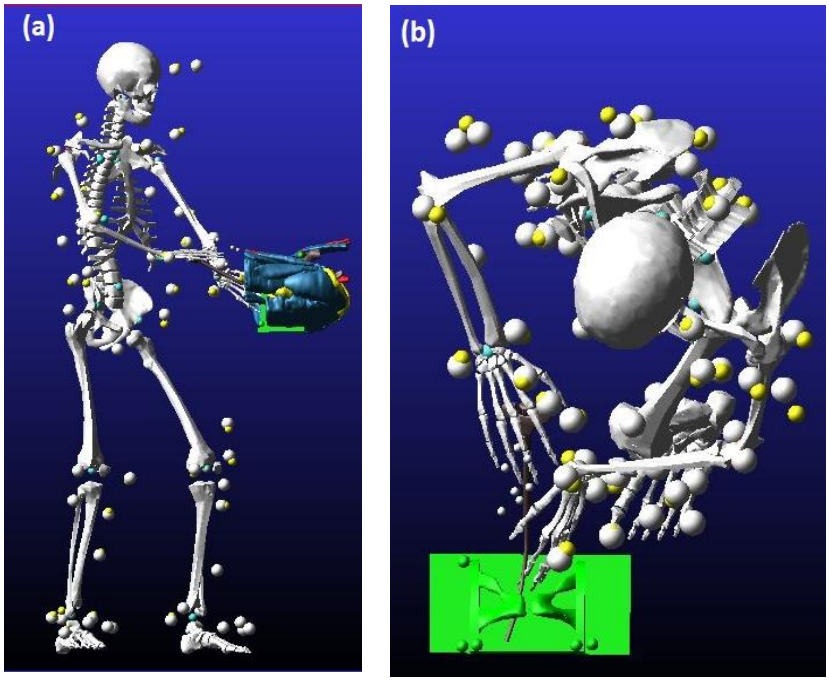

Figure 30: Cephalad deviation: End of trocar passage, surgeon releases the trocar (a) Surgeon kinematics, (b) Instrument kinematics

Figures 27-30 show 4 distinct time steps present in cephalad deviation in which the surgeon tries to puncture the bowel. Retropubic trocar passage can cause injury to bowel as well as other soft structures proximally when the trocar is directed more cephalad. 4 distinct time steps in cephalad deviation are defined in a similar way as they are defined in the error-free (success) trial, i.e. Time step-1: Trocar passage starts from vaginal skin, phase-1 starts (Figure 27); Time step-2: Trocar tip reaches the inferior side of the pubic bone, end of phase-1 and phase-2 starts (Figure 28); Time step-3: Trocar tip reaches the anterior side of the pubic bone, end of phase-2 and phase-3 starts (Figure 29); Time step-4: End of trocar passage and surgeon releases the trocar, end of phase-3 (Figure 30). Figure 29-30 shows how the trocar path deviates in cephalad displacement from the intended path of the trocar.

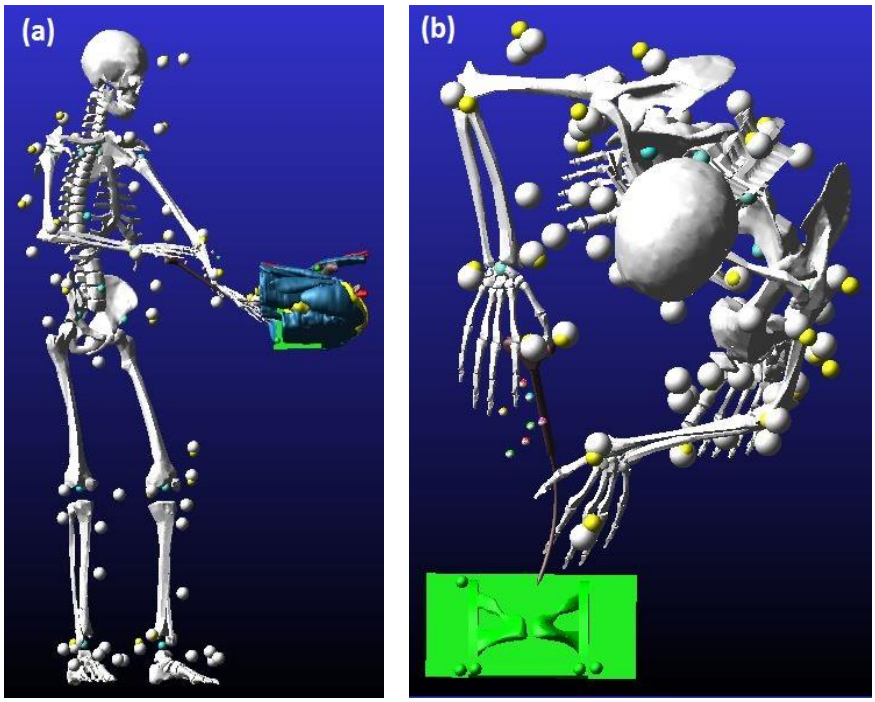

Figure 31: Lateral deviation: Trocar passage starts from skin (a) Surgeon kinematics, (b) Instrument kinematics

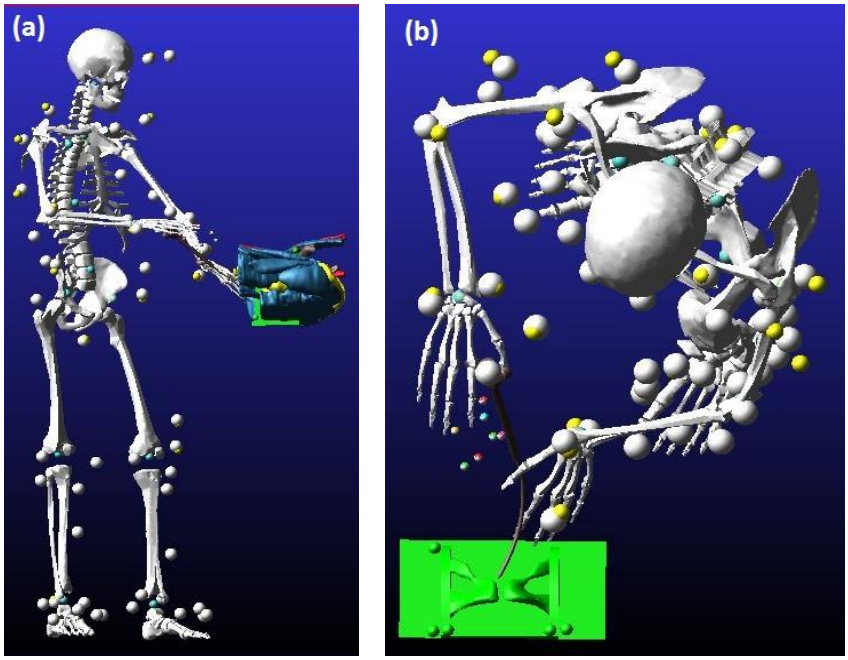

Figure 32: Lateral deviation: Trocar reaches the inferior side of the pelvic bone (a) Surgeon kinematics, (b) Instrument kinematics

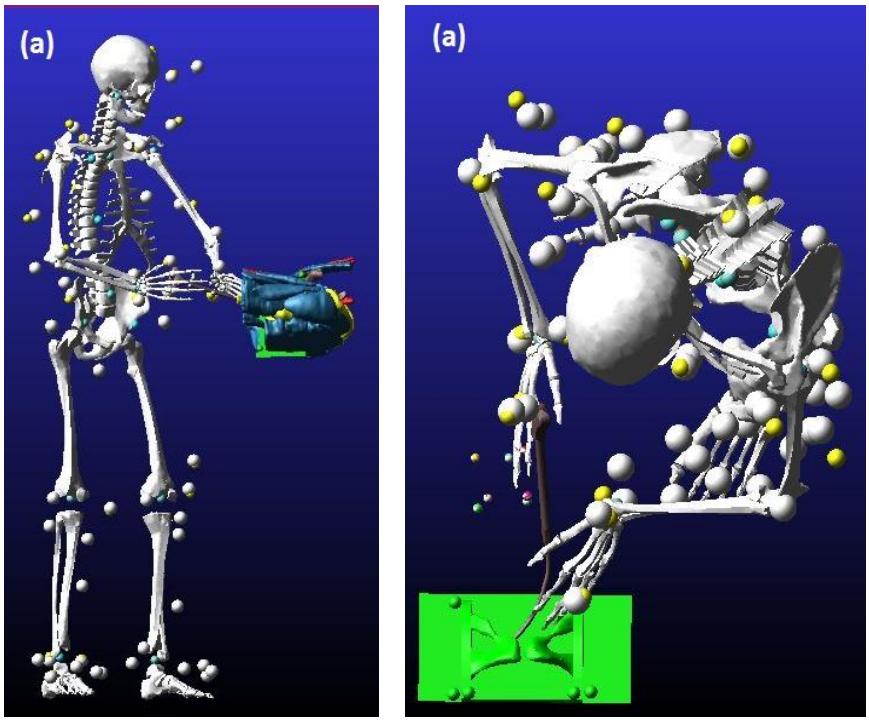

Figure 33: Lateral deviation: End of trocar passage, surgeon releases the trocar (a) Surgeon kinematics, (b) Instrument kinematics

Figures 31-33 show 3 distinct time steps in lateral deviation of trocar where the surgeon tries to puncture the external iliac vein. In lateral deviation of trocar, phase-2 and phase-3 have been merged into a single phase, as the trocar remains within the anterior side of the pubic bone throughout this procedure and therefore, phase-3 was not considered for the lateral deviation of trocar path. 3 distinct time steps and 2 phases of the trocar passage in lateral deviation are defined as follows: Time step-1: Trocar passage starts from the vaginal skin and phase-1 starts (Figure 31); Time step-2: Trocar tip reaches the inferior side of the pubic bone, end of phase-1 and phase-2 starts (Figure 32); Time step-3: Surgeon releases the trocar and end of retropubic trocar passage, end of phase-2 (Figure 33).

5.3 Right Elbow Kinematics

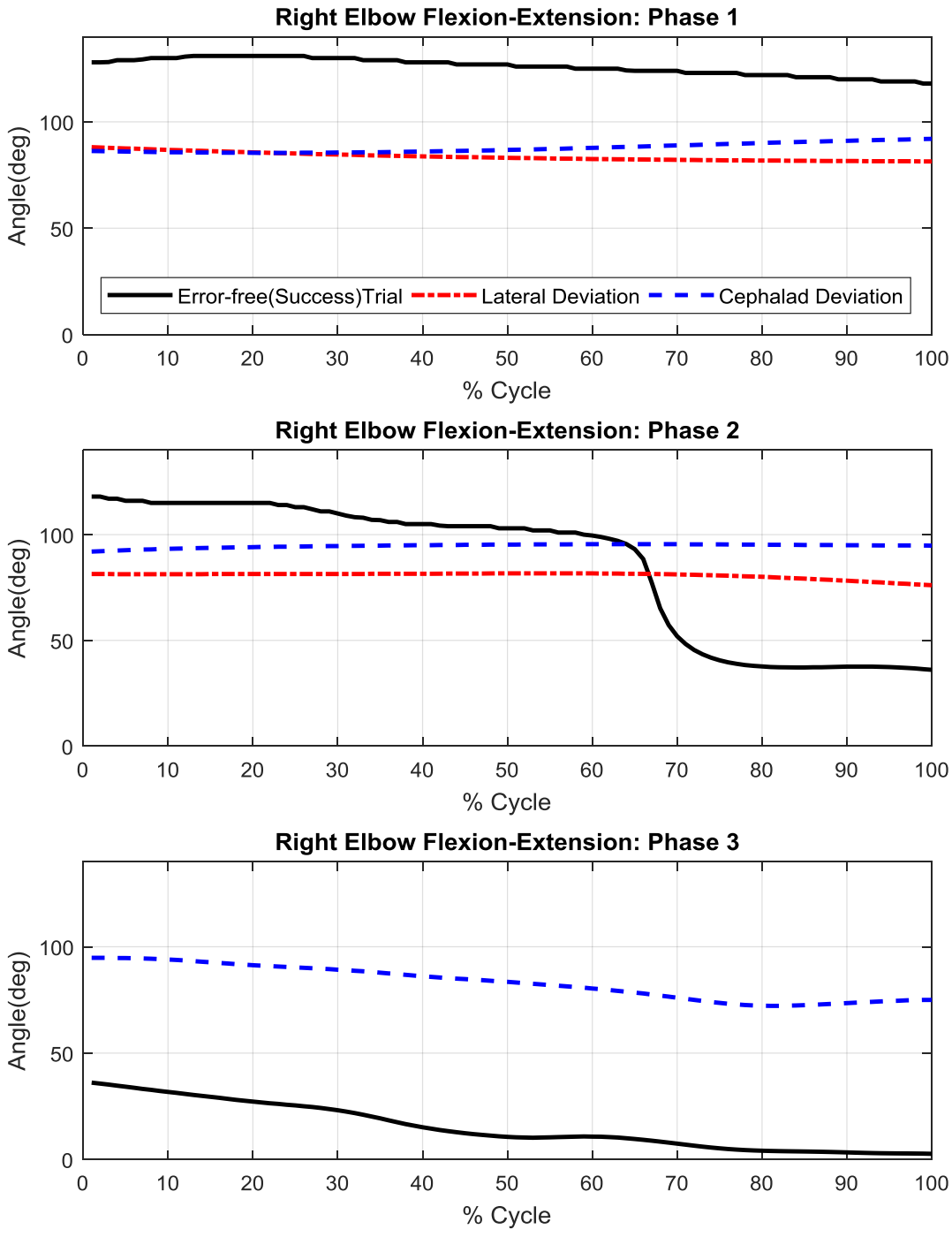

Figure 34: Right Elbow Flexion-Extension

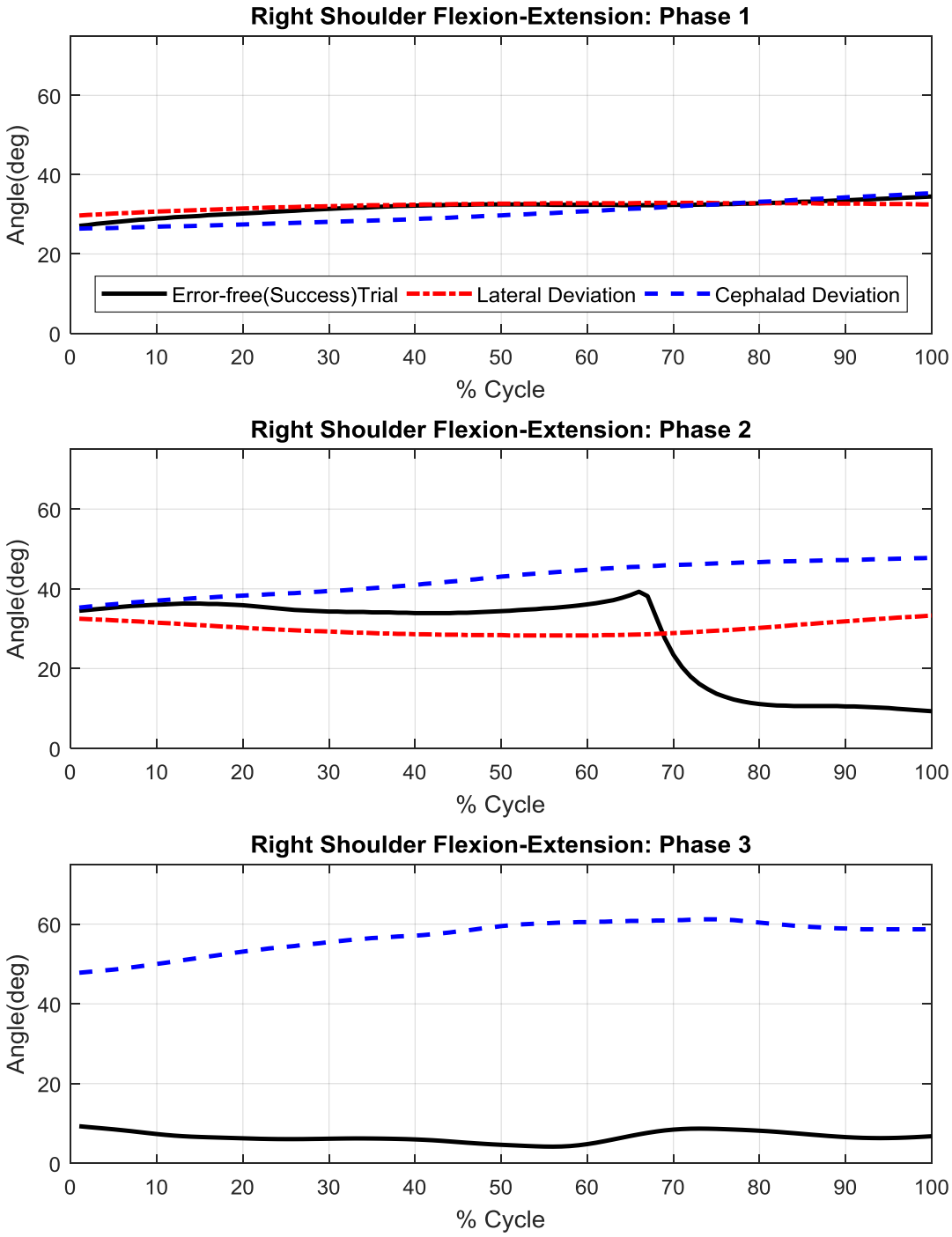

Figure 35: Right Shoulder Flexion-Extension

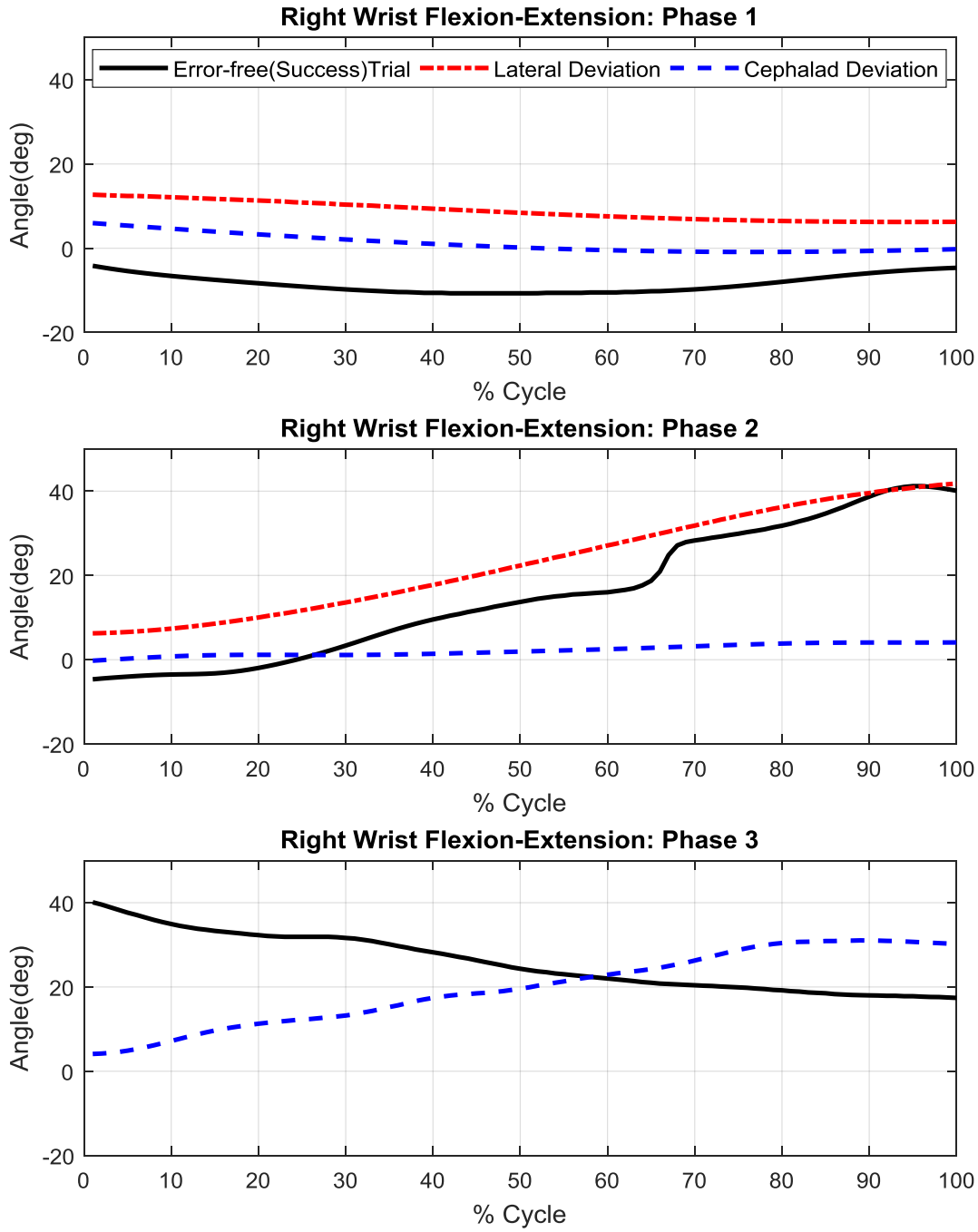

Figure 36: Right Wrist Flexion-Extension

Figures 34-36 provide the flexion-extension angles of right elbow, right shoulder and right wrist joints for error-free (success) trial and error trials (lateral deviation and cephalad deviation). Elbow, shoulder and wrist joint angles have been demonstrated in 3 distinct phases so as to effectively compare between trials (as defined in previous section). In general, phase-1 shows relatively smaller deviation of trocar path between error-free and error trials compared to phase-2 and phase-3 for all three joint angles (elbow, shoulder and wrist joint angles). As previously explained in the figures 32-33 - in lateral deviation of trocar path, surgical trocar remains within the anterior side of the pelvic bone throughout the surgical procedure and therefore, phase-3 only includes the error-free (success) trial and cephalad deviation trial. For both right elbow and right shoulder joints, phase-3 shows greater cephalad deviation than phase-1 and phase-2, while cephalad deviation becomes maximum in phase-2 for right wrist joint.

The range of motion for flexion-extension angles is the highest in error-free (success) trial. Right elbow, shoulder and wrist joint flexion-extension angles are ranged to 128.36 degree, 35.09 degree and 50.8 degree respectively during successful trocar passage.

5.4 Left Elbow Kinematics

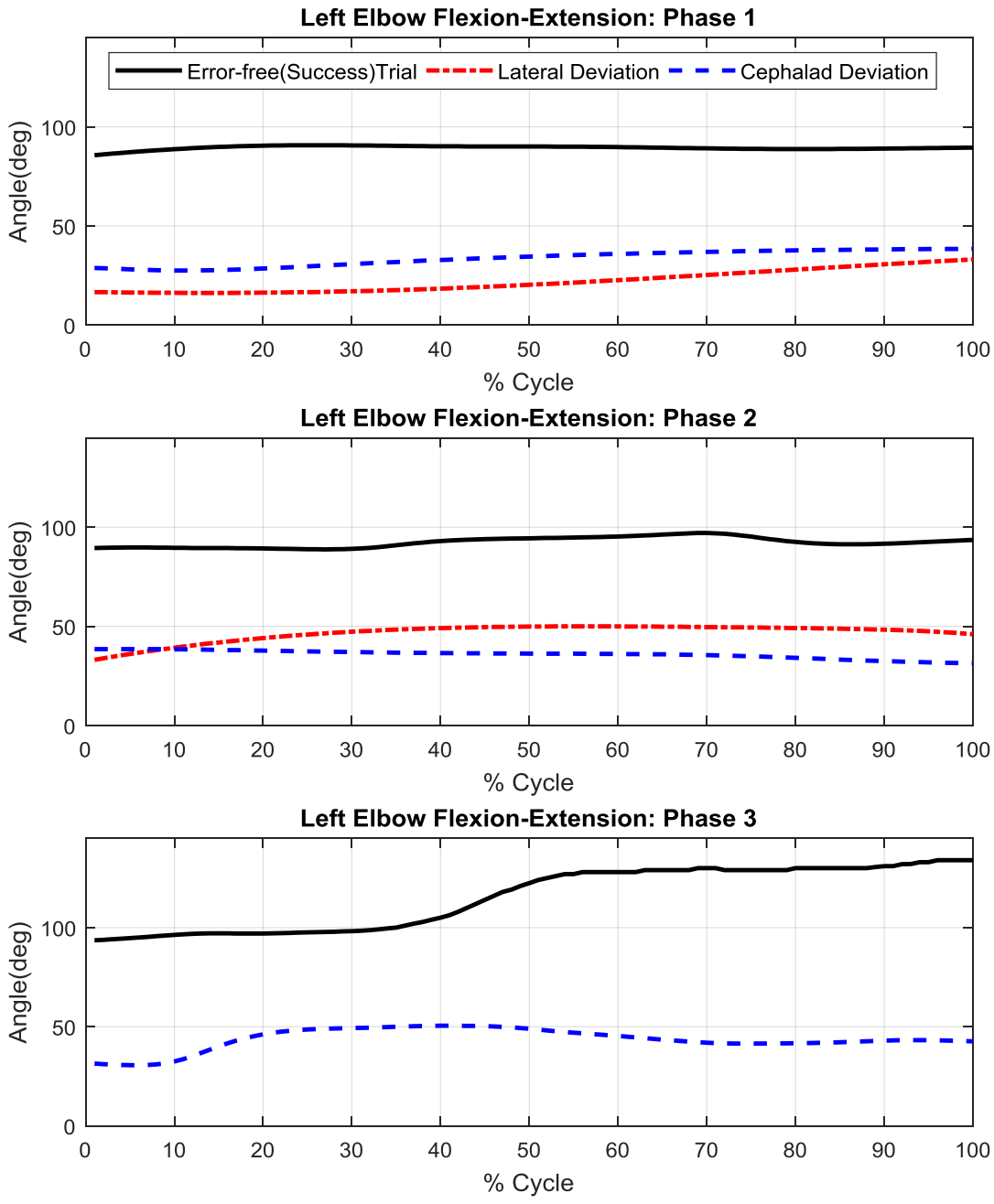

Figure 37: Left Elbow Flexion-Extension

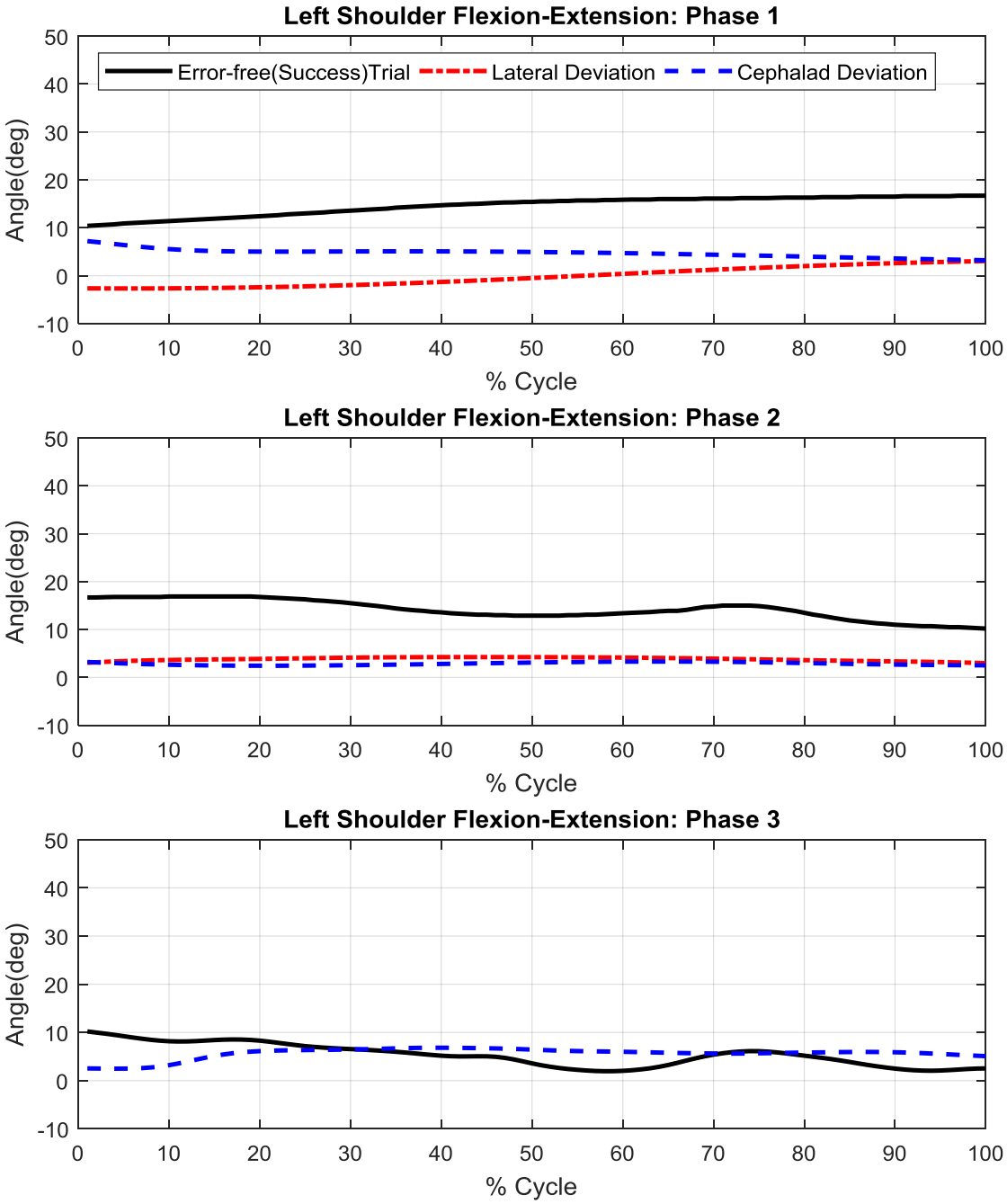

Figure 38: Left Shoulder Flexion-Extension

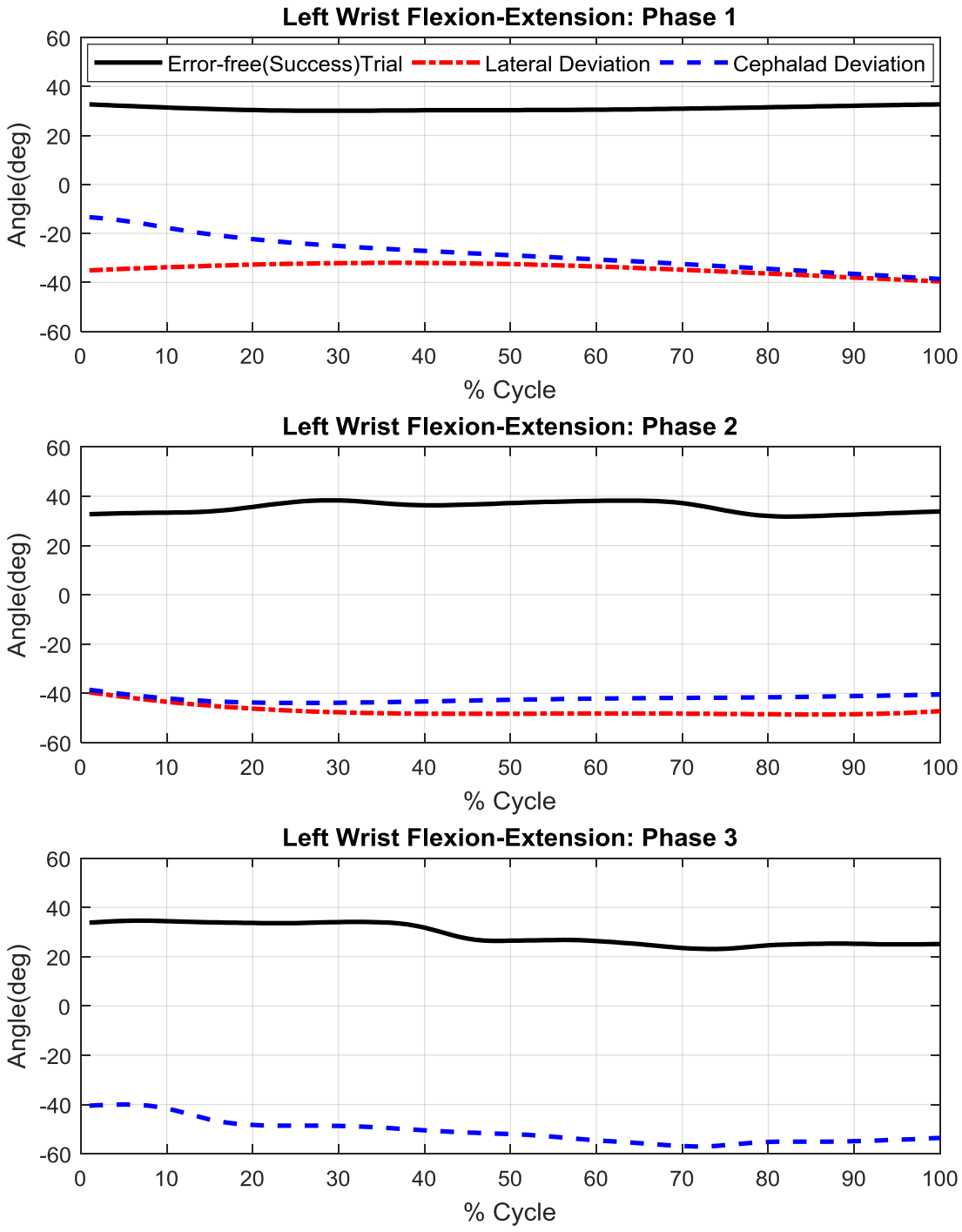

Figure 39: Left Wrist Flexion-Extension

Figures 37-39 provide the flexion-extension angles of left elbow, left shoulder and left wrist joints for error-free (success) trial and error trials (lateral deviation and cephalad deviation). Left elbow, shoulder and wrist joint angles have been demonstrated in 3 distinct phases, similar to the right hand kinematics.

For this experimental setup, left hand served as the auxiliary guiding hand while performing the surgical procedure. Unlike primary guiding hand (right hand) kinematics, auxiliary guiding hand shows relatively higher deviation at phase-1 for left elbow and left shoulder joint flexion-extension angles between error-free and error trials. Cephalad deviation in the left elbow and left wrist joint flexion-extension angles becomes maximum at phase-3, while lateral deviation shows maximum error during phase-1 for left elbow and left shoulder. For both cephalad and lateral deviation, left shoulder deviation becomes maximum at phase-1 which can be attributed to the differences in the initial posture of the surgeon between error-free and error trials. Similar to right hand kinematics, phase-3 was not considered for lateral deviation trials.

The range of motion for flexion-extension angles in left elbow, shoulder and wrist is the highest in error-free (success) trial. Left elbow, shoulder and wrist joint flexion-extension angles are ranged to 48.3 degree, 14.75 degree and 15.2 degree respectively during successful trocar passage.

5.5: RMS Error

The RMS error between the error-free (success) trial and error trials (cephalad deviation and lateral deviation) were calculated to quantify how the trocar path deviates in error trials from the intended trocar path.

Table 2: RMS error quantification of error trials relative to error-free trial: Right hand

Right Elbow			
Trials	Phase-1	Phase-2	Phase-3
Cephalad Deviation	38.4575	33.7866	69.1152
Lateral Deviation	42.4766	32.8138	N/A
Right Shoulder			
Cephalad Deviation	2.1934	18.3985	50.5224
Lateral Deviation	1.7514	11.1143	N/A
Right Wrist			
Cephalad Deviation	11.0159	20.0415	7.8845
Lateral Deviation	17.6509	18.5084	N/A

Table-2 shows the RMS error between error-free (success) trial and error trials in right elbow, right shoulder and right wrist. In cephalad deviation, phase-1 shows relatively smaller RMS errors for right elbow and right shoulder flexion-extension angles and increases gradually from phase to phase, while in lateral deviation, higher RMS errors can be observed from the beginning of the procedure.

Table 3: RMS error quantification of error trials relative to error-free trial: Left Hand

Left Elbow			
Trials	Phase-1	Phase-2	Phase-3
Cephalad Deviation	55.5839	56.4990	72.9339
Lateral Deviation	66.7826	45.5046	N/A
Left Shoulder			
Cephalad Deviation	10.0076	11.4401	2.3932
Lateral Deviation	12.7849	10.4927	N/A
Left Wrist			
Cephalad Deviation	2.1483	7.2308	22.8499
Lateral Deviation	3.5093	12.0447	N/A

Table-3 shows the RMS error between error-free (success) trial and error trials in left elbow, left shoulder and left wrist. Left elbow and left wrist flexion-extension angles in cephalad deviation show relatively smaller RMS error at phase-1 and maximum RMS errors occur at phase-3. Left shoulder flexion-extension angles in cephalad deviation shows relatively higher RMS error from the beginning which can be attributed to the initial differences in posture between error-free and error trials.

In lateral deviation, maximum RMS error in left elbow and left shoulder flexion-extension angle occurs at phase-1, while RMS error increases gradually in left wrist flexion-extension angle.

CHAPTER 6

DISCUSSION

6.1 Analysis of Experimental Results

In order to reduce errors and accelerate the learning experience of surgeons, a novel method has been proposed that can identify, model and prevent surgical errors by using biomechanical motion analysis and a high-fidelity 3-D surgery simulator. Shoulder, elbow and wrist joint motions of surgeon have been analyzed in terms of joint rotations for both error-free and error trials. Flexion-Extension angles for both right and left elbow, wrist and shoulder have been demonstrated in three distinct phases of the procedure. Phase 1: trocar passage from skin to inferior side of the pelvic bone, Phase 2: trocar passage from inferior to anterior side of the pelvic bone, and Phase 3: from anterior side of pelvic bone to end.

For both successful and cephalad deviation (bowel-error) trials, all three distinct phases can be observed. Third phase of this procedure is not evident in the lateral deviation, i.e. iliac-error trial, as the trocar remains within the anterior side of the pelvic bone throughout this procedure once it reaches the pelvic bone. Based on the kinematics of the wrist, elbow, and shoulder joints, differences between the successful and error-trials are more clearly evident during the third phase of the procedure. As the surgeon guides the trocar towards the pubic bone after 1st phase, it enters into the blind space of the pelvic anatomy and differences become more evident between successful and error trials. Differences between trocar trajectories become maximum during the third phase of the procedure, as it goes past the pelvic bone during this period. Surgical errors are more likely to occur during this phase, as the sharp trocar tip becomes more close to the sensitive pelvic

organs during this phase. For this particular experimental setup, an expert surgeon intentionally tries to replicate the error trials here, which might be different in case of actual surgical errors committed by novice surgeons.

Based on the expert surgeon's feedback, the physical model replicated the feeling of performing the procedure on a live subject. The experimental protocol allowed for monitoring of the surgeon's full body kinematics during the procedure, accurate tracking of the trocar inside the body. The kinematics of the wrist, elbow, and shoulder joints demonstrate major differences between the three different passage conditions. Cephalad deviation of the trocar entered the peritoneal cavity, but lateral deviation of the trocar did not result in contact with the external iliac vein. Off plane rotations of the shoulder, elbow and wrist joints, i.e. abduction-adduction, and internal-external rotations, incurred large errors due to the marker set used in the experiment. The kinematics of the wrist, elbow, and shoulder joints demonstrate major differences between the three different passage conditions, indicating that it is possible to identify errors based on kinematics. Since the kinematics between the different trials seem to be different, there is potential in training novice surgeons on proper kinematics to ensure successful passages of the trocar.

Surgical trocar trajectory can be clearly monitored using this novel procedure and thus novice surgeons will be able to get an effective feedback on their expertise level for this particular surgery. Resident surgeons are more prone to surgical errors as they start their surgical career with less experience and skills, and this procedure has the potential to establish a realistic platform for them to practice and get real-time feedback on their performance.

This analysis has been done for one discrete step of this complex and high-risk surgery, but there is potential that this procedure can be translated into other high-risk surgeries to establish a more effective training protocol for novice surgeons.

6.2 Limitations & Improvements

This is a preliminary study with only one expert subject. According to the expert surgeon, creation of the Periurethral tunnels was not similar to that in the operating room, but was successful. The subject tried to replicate error conditions, but it is possible that the kinematics of novice surgeons are different during unintentional error passages. Off plane rotations of the shoulder, elbow and wrist joints, i.e. abduction-adduction, and internal-external rotations, incurred large errors due to the marker set used in the experiment. The ballistic gel was transparent, and the surgeon had to train himself to not visually follow the path of the trocar relative to the bone. This model is missing subcutaneous tissue and skin, although the overall model created operating room-like environment to perform to procedure. The ballistic gel was too dense upon first passage. Upon second and third passes, the density was closer to life like. Through this loss of density, the tunnels had less resistance with each pass, but it never felt like worn tunnels.

The quality of the MUS procedure or the surgeon's performance can be more accurately quantified by monitoring the trocar tip trajectories for different trials and subjects. The distance between the actual and pre-marked trocar exit locations can also be determined to differentiate between trials. Different variables associated with the MUS procedure can also be analyzed, such as time to complete the procedure, trocar tip path

length, distance between the trocar tip and important structures in the pelvic anatomy (bladder, external iliac vein, peritoneum membrane etc.).

6.3 Conclusions

The aim of this procedure is to create a realistic anatomical platform on which surgical trainees can practice their skills and get effective feedback on their overall surgical errors through kinematic analysis. Preliminary study demonstrates the potential of these methods to quantify, and design training protocols for novice surgeon to reduce surgical error in the midurethral sling surgery. In the next phase of the project 25 subjects will be recruited and the kinematics of their upper extremities will be analyzed and classified in terms of surgical experience, successful passages of the trocar and in terms of specific error that can occur.

APPENDIX

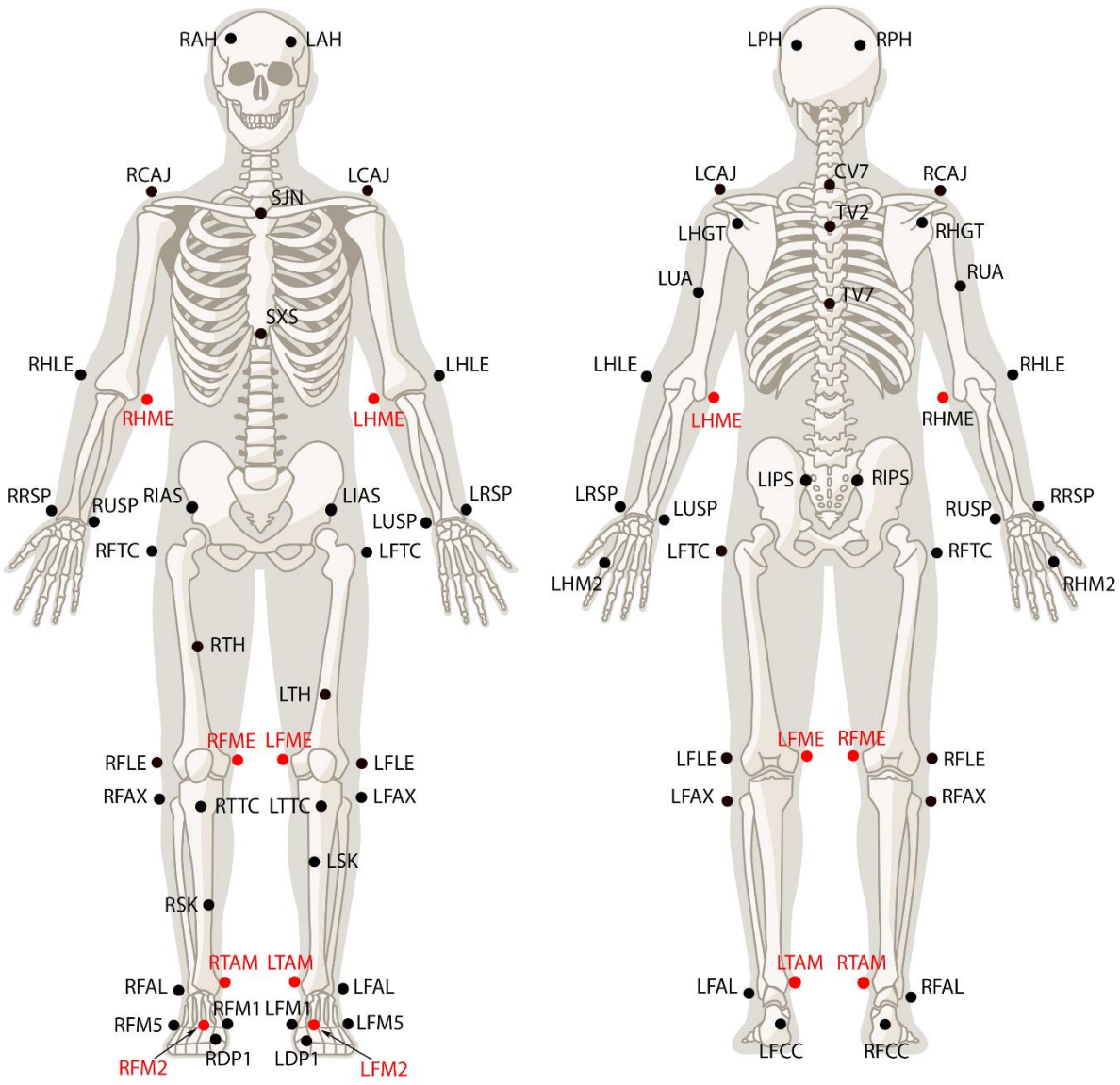

Figure 40: The anterior and posterior views of the Biomech Markerset (57)

Table 4: Marker description for the Biomech Markerset (57)

Section 1: Head Markers

Labels	**Related Segment**	**Anatomical Location**
LAH	Head	Left Anterior Head
RAH	Head	Right Anterior Head
LPH	Head	Left Posterior head
RPH	Head	Right Posterior head

Section 2: Torso Markers

Labels	**Related Segment**	**Anatomical Location**
SJN	Thorax	Sternum Jugular Notch
SXS	Thorax	Sternum Xiphoid Process
CV7	Thorax	Cervical Spine Vertebra 7
TV2	Thorax	Thoracic Spine Vertebra 2
TV7	Thorax	Thoracic Spine Vertebra 7
LHGT	Upper Arm / Shoulder	Left Glenohumeral Joint
RHGT	Upper Arm /Shoulder	Right Glenohumeral Joint

Section 3: Waist Markers

Labels	**Related Segment**	**Anatomical Location**
LIAS	Pelvis	Left Iliac Anterior Spine

RIAS	Pelvis	Right Iliac Anterior Spine
LIPS	Pelvis	Left Iliac Posterior Spine
RIPS		Right Iliac Posterior Spine

Section 4: Upper Extremity Markers

Labels	**Related Segment**	**Anatomical Location**
LCAJ	Thorax	Left Clavicle-Acromion Joint
RCAJ	Thorax	Right Clavicle-Acromion Joint
LHLE	Upper Arm	Left Humerus Lateral Epicondyle
RHLE	Upper Arm	Right Humerus Lateral Epicondyle
LHME	Upper Arm	Left Humerus Medial Epicondyle
RHME	Upper Arm	Right Humerus Medial Epicondyle
LUA	Upper Arm	Left Upper Arm
RUA	Upper Arm	Right Upper Arm

Section 5: Hand Markers

Labels	**Related Segment**	**Anatomical Location**
LHM2	Hand	Left Hand Second metatarsal

RHM2	Hand	Right Hand Second metatarsal
LUSP	Hand	Left Ulna Styloid Process
RUSP	Hand	Right Ulna Styloid Process
LRSP	Hand	Left Radius Styloid Process
RRSP	Hand	Right Radius Styloid Process

Section 6: Lower Extremity Markers

Labels	**Related Segment**	**Anatomical Location**
LFTC	Pelvis	Left Femoral greater Trochanter
RFTC		Right Femoral greater Trochanter
LFLE	Upper Leg	Left Femur Lateral Epicondyle
RFLE		Right Femur Lateral Epicondyle
LFME	Upper Leg	Left Femur Medial Epicondyle
RFME		Right Femur Medial Epicondyle
LTH	Upper Leg	Left Thigh
RTH		Right Thigh

LSK	Upper Leg	Left Superior Knee
RSK		Right Superior Knee
LTTC	Lower Leg	Left Tibial Tubercle
RTTC		Right Tibial Tubercle
LFAX	Lowe Leg	Left Fibula Apex
RFAX		Right Fibula Apex

Section 7: Foot Markers

Labels	**Related Segment**	**Anatomical Location**
LFAL	Lower Leg/Foot	Left Fibula Ankle Lateral
RFAL		Right Fibula Ankle Lateral
LTAM	Lower Leg/Foot	Left Talus Ankle Medial
RTAM		Right Talus Ankle Medial
LFM5	Foot	Left Foot Fifth Metatarsal
RFM5		Right Foot Fifth Metatarsal
LFM2	Foot	Left Foot Second Metatarsal
RFM2		Right Foot Second Metatarsal
LFM1	Foot	Left Foot First Metatarsal
RFM1		Right Foot First Metatarsal
LFCC	Foot	Left Foot Calcaneus
RFCC		Right Foot Calcaneus (Heel)
LDP1	Toes	Left First Distal Phalanx
RDP1	Toes	Right First Distal Phalanx

Table 5: BIOMECH (57) Plugin Marker Set: Motion markers assigned to different body segments

Part	**Marker Name**	**Full Name**
head	RPH	.Model_1.head.RPH
	LPH	.Model_1.head.LPH
	RAH	.Model_1.head.RAH
	LAH	.Model_1.head.LAH
neck	CV7	.Model_1.neck.CV7
Upper_torso	TV2	.Model_1.upper_torso.TV2
	TV7	.Model_1.upper_torso.TV7
	SJN	.Model_1.upper_torso.SJN
	SXS	.Model_1.upper_torso.SXS
Left_scapula	LHGT	.Model_1.left_scapula.LHGT
	LCAJ	.Model_1.left_scapula.LCAJ
Right_scapula	RHGT	.Model_1.right_scapula.RHGT
	RCAJ	.Model_1.right_scapula.RCAJ
Left_upper_arm	LHLE	.Model_1.left_upper_arm.LHLE
	LHME	.Model_1.left_upper_arm.LHME
	LUA	.Model_1.left_upper_arm.LUA
Right_upper_arm	RHLE	.Model_1.right_upper_arm.RHLE
	RHME	.Model_1.right_upper_arm.RHME
	RUA	.Model_1.right_upper_arm.RUA
Left_lower_arm	LUSP	.Model_1.left_lower_arm.LUSP

	LRSP	.Model_1.left_lower_arm.LRSP
Right_lower_arm	RUSP	.Model_1.right_lower_arm.RUSP
	RRSP	.Model_1.right_lower_arm.RRSP
Left_hand	LHM2	.Model_1.left_hand.LHM2
Right_hand	RHM2	.Model_1.right_hand.RHM2
Lower_torso	RIAS	.Model_1.lower_torso.RIAS
	LIAS	.Model_1.lower_torso.LIAS
	RIPS	.Model_1.lower_torso.RIPS
	LIPS	.Model_1.lower_torso.LIPS
Left_upper_leg	LFME	.Model_1.left_upper_leg.LFME
	LFLE	.Model_1.left_upper_leg.LFLE
	LFTC	.Model_1.left_upper_leg.LFTC
	LTH	.Model_1.left_upper_leg.LTH
Right_upper_leg	RFME	.Model_1.right_upper_leg.RFME
	RFLE	.Model_1.right_upper_leg.RFLE
	RTH	.Model_1.right_upper_leg.RTH
	RFTC	.Model_1.right_upper_leg.RFTC
Left_lower_leg	LFAL	.Model_1.left_lower_leg.LFAL
	LSK	.Model_1.left_lower_leg.LSK
	LTTC	.Model_1.left_lower_leg.LTTC
	LFAX	.Model_1.left_lower_leg.LFAX
Right_lower_leg	RFAL	.Model_1.right_lower_leg.RFAL
	RSK	.Model_1.right_lower_leg.RSK

	RTTC	.Model_1.right_lower_leg.RTTC
	RFAX	.Model_1.right_lower_leg.RFAX
Left_foot	LTAM	.Model_1.left_foot.LTAM
	LFCC	.Model_1.left_foot.LFCC
	LDP1	.Model_1.left_foot.LDP1
	LFM5	.Model_1.left_foot.LFM5
	LFM2	.Model_1.left_foot.LFM2
	LFM1	.Model_1.left_foot.LFM1
Right_foot	RTAM	.Model_1.right_foot.RTAM
	RFCC	.Model_1.right_foot.RFCC
	RDP1	.Model_1.right_foot.RDP1
	RFM5	.Model_1.right_foot.RFM5
	RFM2	.Model_1.right_foot.RFM2
	RFM1	.Model_1.right_foot.RFM1

REFERENCES

Aim, F., Lonjon, G., Hannouche, D., and Nizard, R. 2015. Effectiveness of virtual reality training in orthopedic surgery. *Arthroscopy*, 32(1):224-32.

Blaivas, J. G. 2015. Safety considerations for synthetic sling surgery. *Nat Rev Urol*, 12(9): 481-509.

Borchard, A., Schwappach, D. L., Barbir, A., and Bezzola, P. 2012. A systematic review of the effectiveness, compliance, and critical factors for implementation of safety checklists in surgery. *Ann Surg*, 256(6): 925-33.

Catchpole, K. 2010. Errors in the operating theatre—how to spot and stop them. *J Health Serv Res Policy*, 15:48-51

Cristancho, S. M., Hodgson, A. J., Panton, O. N., Meneghetti, A., Warnock, G., and Qayumi, K. 2009. Intraoperative monitoring of laparoscopic skill development based on quantitative measures. *Surg Endosc*, 23(10): 2181-90

Cohn L. T., Corigan J. M., and Donaldson M. S. 2000. Institute of medicine committee on quality of health care in, A., in to err is human: building a safer health system. National Academies Press (US), Washington (DC).

Cuschieri, A. 2005. Reducing errors in the operating room: surgical proficiency and quality assurance of execution. *Surg Endosc*, 19(8): 1022-7.

Ford, A. A. 2015. Mid-urethral sling operations for stress urinary incontinence in women. *Cochrane Database Syst Rev*, (7): Cd006375.

Gawande, A. A. 2003. Analysis of errors reported by surgeons at three teaching hospitals. *Ann Surg*, 133(6): 614-21.

Geraghty, A. 2005. Reducing errors in the operating room: surgical proficiency and quality assurance of execution. *Surg Endosc*, 19(8): 1022-7.

Guess, T. M. and Stylianou, A. P. 2012. Simulation of anterior cruciate ligament deficiency in a musculoskeletal model with anatomical knees. *Open Biomed Eng J*, 6: 23-32.

Hanto, D. W. 2014. Patient safety begins with me. *Ann Surg*, 260(6): 971-2.

Hassinger, J. P. 2010. Virtual pelvic anatomy simulator: a pilot study of usability and perceived effectiveness. *J Surg Res*, 161(1): 23-7.

Hwang, H., Lim, J., Kinnaird, C., Nagy, A. G., Panton, O. N., Hodgson, A. J., and Qayumi, K. A. 2006. Correlating motor performance with surgical error in laparoscopic cholecystectomy. *Surg Endosc*, 20(4): 651-5

James, J. T. 2013. A new, evidence-based estimate of patient harms associated with hospital care. *J Patient Saf,* 9(3): 122-8.

Kirby, G. S., Guyver, P., Strickland, L., Alvand, A., Yang, G. Z., Hargrove, C., Lo B. P., Rees, J. L. 2015. Assessing arthroscopic skills using wireless elbow-worn motion sensors. *J Bone Joint Surg*, 97(13): 1119-27.

Konchada, V. 2011. The Minnesota pelvic trainer: A hybrid VR/physical pelvis for providing virtual mentorship. *Stud Health Technol Inform*, 163: 280-2.

McBeth, P. B., Hodgson, A. J., Nagy, A. G., and Qayumi, K. 2002. Quantitative methodology of evaluating surgeon performance in laparoscopic surgery. *Stud Health Technol Inform*, 85: 280-6.

Moglia, A., Ferrari, V., Morelli, L., Ferrari, M., Mosca F., and Cuschieri, A. 2016. A systematic review of virtual reality simulators for robot-assisted surgery. *Eur Urol*, 69(6): 1065-80.

Rahman, M., Stylianou, A. P. 2016. Lateral collateral ligament deficiency of the elbow joint: A modeling approach. *J Orthop Res*

Siddicky, S. 2015. Use of biomechanical motion analysis to evaluate endotracheal intubation skill in a simulated clinical setting, in Civil and Mechanical Engineering, University of Missouri, Kansas City.

Skoczylas, L. C., Littleton, E. B., Kanter, S. L., and Sutkin, G. 2012. Teaching techniques in the operating room: the importance of perceptual motor teaching. *Acad Med*, 87(3):364-71.

Stylianou, A. P., Guess, T. M., and Kia, M. 2013. Multibody muscle driven model of an instrumented prosthetic knee during squat and toe rise motions. *J Biomech Eng*, 135(4).

Stylianou, A.P., Guess, T. M., and Cook, J. L. 2014. Development and validation of a multi-body model of the canine stifle joint. *Comput Methods Biomech Biomed Engin*, 17(4): 370-7.

Varshney, R. 2014. The McGill simulator for endoscopic sinus surgery (MSESS): a validation study. *Otolaryngol Head Neck Surg,* 43: 40.

Varshney, R. 2014. Development of the McGill simulator for endoscopic sinus surgery: a new high-fidelity virtual reality simulator for endoscopic sinus surgery. *Am J Rhinol Allergy*, 28(4): 330-4.

Wang, D., Zhao, S., Li, T., Zhang, Y., and Wang, X. 2015. Preliminary evaluation of a virtual reality dental simulation system on drilling operation. *Biomed Mater Eng*, 26 Suppl 1:S747-56.

WHO guidelines approved by the guidelines review committee, in WHO guidelines for safe surgery 2009: safe surgery safe lives. 2009, World Health Organization: Geneva.

VITA

Md Arifuzzaman Arif was born on February 1st, 1993 at Nilphamari, Bangladesh. He attended Sonaray High school, a local public school and finished his tenth grade in 2007. The same year, he enrolled at the Notre Dame College and graduated with "outstanding honors" in 2009. The following year, he entered in the Khulna University of Engineering and Technology (KUET) and began studying mechanical engineering. In the spring of 2014, he graduated with a Bachelor of Science degree in Mechanical Engineering.

After finishing the graduation, he joined Institute of Marine Technology, Sirajganj, Bangladesh as an Instructor in Mechanical Engineering. After getting admission in University of Missouri-Kansas City in summer 2016 semester, he moved to the United States and started pursuing his M.S in Mechanical Engineering, with an emphasis in Biomechanics.

In summer 2016, Arif joined the Musculoskeletal Biomechanics Research Laboratory as a graduate research assistant and started working under the direction of Dr. Antonis Stylianou. His experience lies in the area of biomechanical motion analysis, finite element analysis, multibody modeling, CAD, medical image segmentation & 3D modeling, experiment of cadaver specimens, statistical analysis, computer programming etc. His current research is on identification and prevention of pelvic surgical errors using virtual pelvic surgery simulator and Biomechanical motion analysis. Upon completion of his degree requirements for a Master of Science degree in Mechanical Engineering, Arif plans to continue his PhD under the direction of Dr. Antonis Stylianou and have a career in biomechanics.